Measurement of a hyperfine-induced spin-exchange frequency shift in atomic hydrogen

Ronald L. Walsworth* and Isaac F. Silvera
Lyman Laboratory of Physics, Harvard University, Cambridge, Massachusetts 02138

Edward M. Mattison and Robert F. C. Vessot
Harvard-Smithsonian Center for Astrophysics, Cambridge, Massachusetts 02138
(Received 18 November 1991)

We have measured a hyperfine-induced spin-exchange frequency shift in the atomic-hydrogen ground-state hyperfine transition. A recent quantum-mechanical treatment of low-energy hydrogen-hydrogen scattering by Koelman *et al.* [Phys. Rev. A **38**, 3535 (1988)] predicts such frequency shifts to become large at low temperature, and to affect the performance of atomic clocks such as the cryogenic hydrogen maser. The experiment reported here was performed with a hydrogen maser operating near room temperature, where the reported hyperfine effects are predicted to be small, but measurable. Using an adiabatic fast passage (AFP) technique to vary the incoming atomic population in the masing states from approximately 100% (AFP on) to 50% (AFP off), we determined the change in the dimensionless hyperfine-induced frequency-shift parameter Ω to be $\Omega_{on}-\Omega_{off}=5.38\ (1.06)\times10^{-4}$. The theoretical prediction at this temperature is $\Omega_{on}-\Omega_{off}=-0.76\times10^{-4}$ to -1.12×10^{-4}, for the range of masing-state populations used in the present experiment. We review the relevant theory, report our experimental method and results, and discuss possible reasons for the discrepancy between experiment and theory.

PACS number(s): 34.20.Cf, 34.40.+n, 42.52.+x

I. INTRODUCTION

The atomic-hydrogen (H) maser is the most stable time and frequency standard currently available for measurement intervals between 1 and 10^4 sec. The fractional frequency stability of state-of-the-art H masers, such as those designed and constructed by the Harvard-Smithsonian Center for Astrophysics (CfA) maser group [1], is typically better than one part in 10^5 for averaging intervals of 10^4 sec. The H maser is an essential frequency reference for radio astronomy, and is used as a highly stable clock for time keeping, for worldwide navigation, and for precision tests of gravitation [2], relativity [3], and quantum mechanics [4]. In addition, it is a valuable instrument for experimental atomic and condensed matter physics [5], including work at low temperatures [6–8].

In 1978 Crampton, Phillips, and Kleppner [9] pointed out that a cryogenic H maser could have improved frequency stability due to a reduced H-H spin-exchange relaxation rate at low temperature and the resulting higher operational signal power. Further analyses [10,11] indicated that a cryogenic H maser might have a frequency stability 2 to 3 orders of magnitude better than room-temperature H masers. In 1980 the possibility of a cryogenic H maser working below 1 K became a reality when Silvera and Walraven [12] stabilized atomic hydrogen by storing the atoms in a container with superfluid helium-covered walls, to suppress the wall adsorption and subsequent recombination of H into molecular H_2. In 1986 three groups [6–8], including ours, demonstrated oscillation of a cryogenic H maser using such superfluid helium-lined containers.

Spin exchange is a ubiquitous process in low-energy collisions between particles with spin (atoms, ions, electrons), and is typically well described by an exchange interaction that operates during the time of collisional close approach. Spin exchange can change the spin quantum numbers of the colliding particles and thereby cause relaxation among spin-state populations as well as frequency shifts in the transitions between the spin states. These relaxation rates and frequency shifts depend sensitively on the interaction potentials of the colliding particles.

Early treatments of spin-exchange effects for ground-state H-H collisions assumed a degenerate-internal-states (DIS) model, in which hyperfine interactions are ignored relative to the electron exchange interaction during the collision [13–20]. Such an assumption seems reasonable at room temperature, since the energy of the H ground-state hyperfine interaction ($\sim$0.07 K) is very small relative to the maximum depth of the electron exchange potential ($\sim$50 000 K) and the collisional kinetic energy. Indeed, good agreement has been found between the predictions of the DIS theory and the measurement [21,22] of spin-exchange-induced relaxation rates and frequency shifts in room-temperature H masers [23,24]. Nevertheless, including the hyperfine interaction in an analysis of H spin exchange is important because it fundamentally alters the rotational symmetry of the scattering problem. For very-low-energy collisions, where the kinetic energy becomes comparable to the hyperfine interaction energy, such considerations may be particularly significant.

In 1975 Crampton and Wang (CW) initiated the study of *hyperfine-induced* (HI) spin-exchange effects in H-H collisions with a semiclassical treatment of the problem [25]. Their analysis predicted a hyperfine-induced spin-exchange frequency shift, the HI shift, with a calculated

value found to be in reasonable agreement with measurements CW made near room temperature with a H maser. Recent calculations by Verhaar, Koelman, Stoof, Luiten, and Crampton (VKSLC) [26,27] have included the hyperfine interaction in a fully quantum-mechanical analysis of H-H spin-exchange collisions. VKSLC found that the HI shift in H greatly increases in magnitude as the temperature (T) of the atomic gas is lowered, until the HI shift becomes the dominant spin-exchange frequency shift for $T < 10$ K . In the VKSLC theory consideration of both the electron and the nuclear spin identities is essential, because the hyperfine interaction couples these spins and thereby changes the rotational symmetry of the collision problem. This results in the HI frequency shift, with a unique dependence upon the population of the atomic hyperfine states; such a dependence is *not* given by the semiclassical treatment due to CW. The VKSLC calculations indicated that the HI shift at low temperatures is surprisingly sensitive to nonadiabatic effects and to the details of the H-H interaction potential at long range. In practice, the magnitude of the HI shift and its dependence on the atomic-state distribution may make it more difficult to achieve the predicted [9–11] radical improvement in frequency stability using a cryogenic H maser. It is also possible that analogous HI shifts in alkali-metal gases such as sodium [28] and cesium [29,30] may limit the performance of atomic fountain clocks that employ laser-cooling techniques [31,32].

In the experiment reported in the present paper we measured the dependence of the hydrogen HI shift on the atomic hyperfine state distribution, near room temperature. The experiment was performed with a H maser built at CfA, and used an adiabatic fast passage (AFP) technique to vary the incoming atomic population in the two masing states between approximately 100% (AFP on) and 50% (AFP off). We determined the change in the HI frequency-shift parameter Ω to be $\Omega_{\rm on}-\Omega_{\rm off}=5.38\ (1.06)\times10^{-4}$. The VKSLC prediction at this temperature is $\Omega_{\rm on}-\Omega_{\rm off}=-0.76\times10^{-4}$ to -1.12×10^{-4}, for the range of masing-state populations used in the present experiment. Thus the experimental result reported here significantly disagrees with the calculation by VKSLC. We have not identified a likely cause of this discrepancy. Nevertheless, the present experiment is significant in four respects: (i) it confirms a dependence of the H HI shift on the atomic hyperfine state distribution, as predicted qualitatively by VKSLC; (ii) it tests the accuracy of this quantum-mechanical HI theory, specifically the calculational techniques and the interatomic potentials that were used, knowledge that is fundamental to understanding low-energy atomic collisions; (iii) it allows a better assessment of the impact that HI shifts could have on room-temperature H maser frequency stability; and (iv) it reflects upon the confidence one can have in the VKSLC predictions of large HI frequency shifts at low temperatures.

The remainder of this paper is organized as follows. Section II reviews both the semiclassical (CW) HI theory and the quantum-mechanical (VKSLC) theory, especially as they pertain to our experiment. Section III gives an overview of the apparatus and techniques used in the present experiment. In Sec. IV our data are presented and interpreted in terms of the VKSLC frequency-shift model. In Sec. V the experimental result is compared with the theoretical prediction, and possible reasons for the discrepancy between the two are investigated. Finally, the significance of this experiment and relevant work in progress are discussed in Sec. VI.

II. REVIEW OF THEORY

A. Semiclassical theory

The semiclassical treatment of the atomic hydrogen (H) hyperfine-induced (HI) spin-exchange frequency shift is due to Crampton and Wang (CW) [25]. They considered the hyperfine interaction to be "interrupted" during a H-H collision when the electron exchange interaction can be thought of as "strong." Repeated, brief interruptions of the phase evolution of the atomic hyperfine coherence, caused by such H-H collisions, lead to a negative frequency shift of the hyperfine transition that is proportional to the collision rate. CW evaluated this H phase evolution by assuming that the two atomic nuclei involved in a binary collision follow undeflected straight-line paths; they then integrated over all input angles (impact parameters) and velocities, for a thermal distribution of H atoms in a H maser operating near room temperature. This classical treatment of the nuclear kinetic motion assumes the nuclei to be distinguishable and ignores any acceleration due to the exchange potentials, van der Waals forces, etc.

The time evolution of the atomic spin states is taken to be governed by the Hamiltonian

$$H(t)=E_T(t)P_T+E_S(t)P_S+V_{\rm hf}\ , \tag{1}$$

where $E_{S(T)}(t)$ are the singlet- (triplet-) state H-H interaction energies, $P_{S(T)}$ are the singlet- (triplet-) state H-H electron spin projection operators, and $V_{\rm hf}$ is the sum of the *intra*-atomic H hyperfine interactions:

$$V_{\rm hf}=\hbar\omega_{\rm hf}(\mathbf{I}_1\cdot\mathbf{S}_1+\mathbf{I}_2\cdot\mathbf{S}_2)\ . \tag{2}$$

Note that the time dependence of $E_{S(T)}(t)$ and thus of $H(t)$ comes from the motion of the two H nuclei, changing the internuclear separation and thereby determining the strength of the electron exchange interaction. The Schrödinger equation was solved numerically for $H(t)$ using time-dependent perturbation theory, with $E_TP_T+E_SP_S$ taken to be the unperturbed Hamiltonian and $V_{\rm hf}$ included only to first order (the first-order Born approximation). Labeling the H hyperfine levels a, b, c, and d in order of increasing energy (see Fig. 1), it is the $c\rightarrow a$ transition on which a H maser typically operates (frequency $\approx$1420 MHz). The semiclassical CW calculation found the frequency shifts to the c-a transition to be

$$\omega-\omega_0=[\Delta_c+\alpha\bar{\lambda}_0^{\rm sc}]\gamma_2-\Omega_{\rm sc}\gamma_{\rm H}\ . \tag{3}$$

Here ω is the maser's output frequency and ω_0 is the atomic resonance frequency including the Zeeman shift of the hyperfine energy levels, a shift due to H collisions with the walls of the maser storage bulb (typically coated

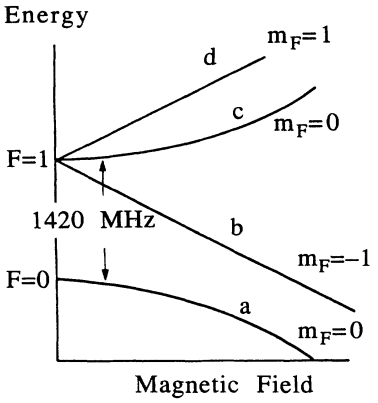

FIG. 1. The hydrogen hyperfine energy levels in the ground electronic state, as a function of applied magnetic field.

with Teflon) [23,24], and the second-order Doppler shift. The parameter $\Delta_c \approx (2Q_c/\omega_0)(\omega_c-\omega_0)$ represents the cavity pulling of the maser frequency, where ω_c is the maser cavity's resonance frequency and Q_c is its quality factor. The parameter γ_2 is the atomic dephasing rate (proportional to the total atomic linewidth) and γ_H is the portion of γ_2 resulting from H spin-exchange relaxation (proportional to the H density). The product $\alpha\bar{\lambda}_0^{sc}$ is only slightly modified from the spin-exchange frequency shift predicted by the degenerate-internal-states (DIS) treatment [20], with α equal to the relative atomic velocity times a system constant. Finally, Ω_{sc} is the *semiclassical HI spin-exchange frequency-shift parameter* ($=-\varepsilon_H$ in the notation used by CW [25]).

In the semiclassical theory of CW the HI shift does not depend upon the atomic hyperfine state populations (ρ_{cc}, ρ_{aa}, etc). Thus Ω_{sc} is just a constant for a given temperature. CW's numerical calculation found $\Omega_{sc}=3.57\times10^{-4}$ at $T=308$ K, the temperature at which the CW experiment was performed. As will be seen in Sec. II B below, the quantum-mechanical theory [26,27] predicts the general HI shift parameter Ω to be a function of the state populations. Note that in experiments using H masers, first CW [25] and then Elkin and Zhestkova [33] determined a value for Ω_{sc} in reasonable agreement with CW's semiclassical calculation.

B. Quantum-mechanical (VKSLC) theory

In this section we review the quantum-mechanical theory of H HI spin-exchange effects, due to Verhaar, Koelman, Stoof, Luiten, and Crampton (VKSLC) [26,27]. The VKSLC theory begins with the time evolution equation for the H hyperfine density matrix, a quantum-mechanical Boltzmann equation for a homogeneous system. Included is a Hamiltonian term for coherent interaction with radiation, as in a H maser; a phenomenological relaxation term to account for all one-atom processes that destroy coherences and/or change the hyperfine state populations; and a binary collision term to account for all spin-exchange effects. VKSLC addressed conditions typical for a H maser: sufficiently low H density so that only binary collisions need to be considered; and a single coherence between the four hyperfine levels, namely, between the c and a states (see Fig. 1).

VKSLC used the same collision interaction Hamiltonian as in the semiclassical CW theory [see Eqs. (1) and (2)], but employed more modern and improved potentials for the exchange interaction. The collision term for the evolution of the c-a coherence (ρ_{ac}) is taken to be

$$\left.\frac{d\rho_{ac}}{dt}\right|_{\text{collision}} = n\bar{v}\rho_{ac}\sum_{\nu}\bar{G}_{\nu}\rho_{\nu\nu}\ , \tag{4}$$

where n is the H density, $\bar{v}$ is the thermally averaged relative collision velocity, and the $\bar{G}_{\nu}$ are thermally averaged complex "cross sections" that describe both the spin-exchange frequency shift (imaginary part) and the coherence relaxation (real part). (The overbar refers to thermal averaging.) The sum runs over all four of the hyperfine levels (a,b,c,d) so, in general, the spin-exchange shift and relaxation effects are described by four cross sections each. These complex cross sections can be given in terms of elastic $\underline{S}$-matrix elements as

$$G_{\nu}(E_k)=\frac{\pi}{k^2}\sum_{l}(2l+1)[\underline{S}^{\,l}_{\{a\nu\}\{a\nu\}}(E_k) \times\underline{S}^{\,l*}_{\{c\nu\}\{c\nu\}}(E_k)-1]\ , \tag{5}$$

where E_k is the center of mass kinetic energy and l is the two-body angular momentum quantum number (the partial wave number), while the two subscripts between brackets are a shorthand notation for normalized (anti)symmetric two-body spin states for the (odd) even values of l. Note that antisymmetric spin states can only be formed simultaneously for $\{a\nu\}$ and $\{c\nu\}$ with $\nu=b$ or d; similarly, the only symmetric spin states that contribute to G_{ν} have $\nu=c$ or a, as all other symmetric spin states have unmixed $S=1$ (in the zero magnetic field limit [34]) and so the $\underline{S}$-matrix products within G_{ν} are canceled by the corresponding factors of -1. Therefore the $\nu=b$ or d terms in G_{ν} have contributions from odd l only, while the $\nu=c$ or a terms have even l only.

The general expression for the c-a coherence collision term, as given in Eqs. (4) and (5), can be simplified and more easily understood by considering the rotational symmetry of the H-H collision problem. Including the exchange and hyperfine interactions, as in Eqs. (1) and (2), the collision Hamiltonian has $SO(3)_{orbit}\otimes SO(2)_{spin}$ as a symmetry group: the direct product of the three-dimensional rotation group for the two-atom orbital angular momentum with the two-dimensional atomic spin rotation group about the z axis (parallel to the static magnetic field). Due to the SO(3) orbital symmetry the $\underline{S}$-matrix elements are diagonal in the angular momentum quantum number l (and independent of m_l). This is already taken into account in Eq. (5) above. Because of the SO(2) spin symmetry the total atomic spin magnetic quantum number m_F is conserved. It directly follows that only elastic $\underline{S}$-matrix elements are allowed for odd l; that is, spin-exchange collisions between atoms participating in the c-a coherence and atoms in the state $\nu=b$ or d interact with odd l only, but do not change $b\leftrightarrow d$ ($\Delta m_F\neq0$).

In the zero magnetic field limit [34], and *including the hyperfine interaction,* there is the additional symmetry that the effect of a H-H spin-exchange collision on the *c-a* coherence is unchanged by a 180° rotation of *both* the electron and proton spins about any axis in the *x-y* plane ($m_S \rightarrow -m_S$ and $m_I \rightarrow -m_I$ for electron spin S and nuclear spin I). Such a rotation takes the *b* state $\rightarrow$*d* state, and similarly $d \rightarrow b$, while $a \rightarrow a$ and $c \rightarrow c$. (Thus the symmetric two-atom spin states *aa*, *cc*, and $\{ac\}$ remain invariant under the 180° rotation.) Combined with the conservation of the quantum number m_F, this symmetry allows only elastic $\underline{S}$-matrix elements for even l; that is, spin-exchange collisions between atoms participating in the *c-a* coherence and atoms in the state $v=a$ or c interact with even l only, but cannot change $a \leftrightarrow c$. The 180° rotation symmetry also leads to degeneracies among the various shift and broadening cross sections: for the *c-a* coherence of interest here one finds $G_b = G_d$ (see Table I).

The effect of H-H collisions on the *c-a* coherence can be analyzed in terms of a spin-exchange frequency shift ($\Delta\omega_H$) and relaxation (γ_H).

Substituting $\rho_{ac}(t) = \rho_{ac}(0)[i\Delta\omega_H - \gamma_H]t$ into Eq. (4), including the degeneracy $G_b = G_d$, and using a slowly varying amplitude approximation, one finds

$$\Delta\omega_H = n\bar{v}[\bar{\lambda}_0(\rho_{cc}-\rho_{aa})+\bar{\lambda}_1(\rho_{cc}+\rho_{aa})+\bar{\lambda}_2] , \quad (6)$$

$$\gamma_H = n\bar{v}[\bar{\sigma}_0(\rho_{cc}-\rho_{aa})+\bar{\sigma}_1(\rho_{cc}+\rho_{aa})+\bar{\sigma}_2] , \quad (7)$$

where the HI spin-exchange frequency-shift cross sections (λ's) are given by

$$\lambda_0 \equiv \mathrm{Im}\left[\frac{G_c - G_a}{2}\right] ,$$

$$\lambda_1 \equiv \mathrm{Im}[\tfrac{1}{2}(G_c+G_a)-G_b] , \quad (8)$$

$$\lambda_2 \equiv \mathrm{Im}(G_b) ,$$

and the HI spin-exchange coherence relaxation cross sections (σ's) are given by analogous expressions in terms of the real parts of the G_v's. Including the radiation terms (Maxwell-Bloch equations) and the one-atom relaxation terms [20], the net H maser frequency predicted by the VKSLC theory becomes

$$\omega - \omega_0 = [\Delta_c + \alpha\bar{\lambda}_0]\gamma_2 - \Omega\gamma_H , \quad (9)$$

where

TABLE I. Degeneracies in spin-exchange cross sections due to the 180° rotation symmetry, for collisions of an *a* or *c* state atom with a *v* state atom ($v=a,b,c,d$). Arrows imply degeneracy.

Including hyperfine interaction	Degenerate internal states
$ab \leftrightarrow ad$	$ab \leftrightarrow ad$
$cb \leftrightarrow cd$	$cb \leftrightarrow cd$
	$aa \leftrightarrow cc$
	$ab \leftrightarrow cb$
	$ad \leftrightarrow cd$

$$\Omega = -\frac{\bar{\lambda}_1(\rho_{cc}+\rho_{aa})+\bar{\lambda}_2}{\bar{\sigma}_1(\rho_{cc}+\rho_{aa})+\bar{\sigma}_2} \quad (10)$$

is the quantum-mechanical HI spin-exchange frequency-shift parameter. [Here the $\bar{\sigma}_0(\rho_{cc}-\rho_{aa})$ term in Ω has been dropped as it is expected to be much smaller than the remaining relaxation terms [27].] Note the dependence of Ω on the masing-state population ($\rho_{cc}+\rho_{aa}$). This implies that the HI shift is nonlinear in the atomic density (n), because the spin-exchange relaxation rate γ_H is linear in n to first order [see Eq. (7)], and ($\rho_{cc}+\rho_{aa}$) depends upon density in a complicated manner due to this same spin-exchange relaxation [see Eq. (11) below]. It is this dependence of the HI shift upon the masing-state population that is tested in the experiment reported in the present paper.

The familiar degenerate-internal-states (DIS) expression for the H spin-exchange frequency shift ignoring the hyperfine interaction [see Eq. (3)] can also be generated using symmetry arguments. In the DIS treatment of H-H collisions the proton spins serve only to label the atomic states, as there is no hyperfine coupling to the electron spins. (The electron spins interact via the exchange interaction). Thus the collision problem is symmetric under a 180° rotation of proton spin about the quantization axis (the direction of the static magnetic field). This exchanges the *a* and *c* states while not affecting the *b* and *d* states. In addition, the 180° rotation symmetry of *both* electron and proton spins remains valid in the absence of the hyperfine interaction. Therefore neglecting the hyperfine interaction in an analysis of H-H spin exchange leads to a greater number of rotational spin symmetries, and hence to a greater number of degeneracies between the general spin-exchange cross sections (G_v's); see Table I for a listing of the cross-section degeneracies in the DIS treatment. This leads to the simpler DIS expression for the H spin-exchange frequency shift [Eq. (3)].

VKSLC have numerically calculated the H HI spin-exchange shift and relaxation cross sections for collision energies from 10^{-3} to 10^{3} K [26,27]. As the singlet and projection operators in the exchange interaction [see Eq. (1)] are not in general diagonal in the H spin-state basis, the coupled radial equations describing the H-H scattering wave functions must be integrated for each of the various channels; e.g., an atom with a *c-a* coherence colliding with a *b* state atom, or a *c* state atom, etc. This is known as a coupled-channel (CC) calculation [35,36], and in principle it can give exact results. VKSLC carried out such a full CC calculation for the cross-section expressions given in Eqs. (5) and (8) above, with H gas temperatures (T) below 50 K.

Since the experimentally relevant parameters are the *thermally (or Boltzmann) averaged* cross sections, it became prohibitive in terms of time and computer usage for VKSLC to perform a complete CC calculation at higher temperatures. Thus they also performed a simpler calculation that includes the hyperfine interaction as a first-order correction to the DIS treatment of H-H spin-exchange collisions. This first-order calculation takes advantage of the fact that the hyperfine interaction is very weak relative to the maximum strength of the exchange

interaction. However, the hyperfine interaction does not fall off at large H-H distances. To account for these effects, VKSLC's first-order calculation consists of a Born-type integral restricted to a finite volume, beyond which the exchange interaction is considered negligible, and a Wronskian surface term to compensate for the infinite extent of the hyperfine interactions [37].

In general, VKSLC found that the CC and first-order calculations agree quite well, so long as it is valid to assume that the hyperfine interaction is a small perturbation during the collision. The first-order calculation can break down when the "collision time" (the time of close internuclear approach) becomes comparable to the phase precession period associated with the hyperfine interaction. This will occur at very low collision energies ($T \lesssim 0.2$ K $\sim 2\hbar\omega_{\rm hf}$) and near narrow scattering resonances. However, since all such narrow resonances occur for collision energies much greater than the hyperfine energy [e.g., the significant $v=11$, $l=13$ resonance has $E(k) \approx 276$ K], VKSLC were able to correct for deviations in their first-order calculation by small zeroth-order shiftings of the DIS H-H internal energy in the vicinity of each troublesome resonance. VKSLC believe that this was sufficient to bring the results back in line with the CC calculations.

VKSLC used "state-of-the-art" singlet and triplet H-H potentials [38–41] in their numerical calculations. These potentials incorporate departures from the Born-Oppenheimer ("clamped nuclei") approximation to first order, a treatment known as the "adiabatic" correction. They also include "nonadiabatic" (second-order) corrections to the bound-state energy levels, and first-order radiative and relativistic corrections. (Note that even better H-H potentials have been developed [42,43] since the VKSLC work.) Additional nonadiabatic corrections to bound states near the continuum, and for the continuum part of the calculation, were accomplished by replacing the reduced nuclear mass $\mu_p = \frac{1}{2}m_p$ with the reduced atomic mass $\mu_{\rm H} = \frac{1}{2}m_{\rm H}$ in the adiabatic radial Schrödinger equation. This technique follows the method of Bunker, McLarnon, and Moss [44]. Interestingly, the numerical results of VKSLC exhibit a remarkable sensitivity to this nonadiabatic correction, at low collision energies. For example, the replacement of $\mu_{\rm H}$ by μ_p, a *0.05% difference,* leads to a change in the HI frequency-shift parameter Ω of roughly a *factor of 2* for $T \lesssim 5$ K. Such extreme sensitivity to nonadiabatic effects is surprising, although it may be related to an enhanced influence of bound vibrational-rotational molecular state resonances close to the continuum on the few partial waves that contribute at low temperatures to H-H scattering [45,46]. This heightened sensitivity to nonadiabatic effects is an example of the interesting and unique physics of cold atomic collisions. (Note that we are currently engaged in a measurement of the HI shift for $T \sim 0.5$ K using a cryogenic H maser [8].)

Relevant results from the numerical calculations of VKSLC are displayed in Figs. 2 and 3. These figures have been published previously by VKSLC [27], but are reproduced here for the convenience of the reader. Figure 2 displays the thermally averaged shift and relaxation

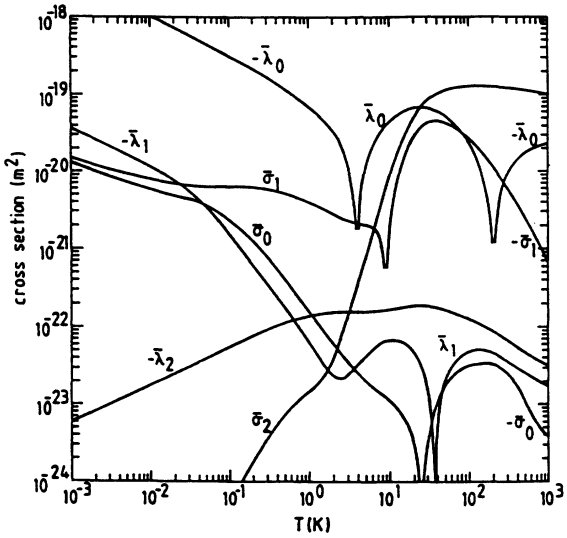

FIG. 2. VKSLC's calculation of the thermally averaged spin-exchange frequency shift (λ's) and broadening (σ's) cross sections for H-H collisions, including the hyperfine-induced terms. (Figure adapted from Ref. [27].)

cross sections as a function of the H gas temperature, for $10^{-3} < T < 10^{3}$ K. All the values shown in Fig. 2 were generated by VKSLC with their first-order calculation. Note that VKSLC's low-energy values for $\bar{\lambda}_0$, $\bar{\sigma}_1$, and $\bar{\sigma}_2$ differ somewhat from past DIS calculations [47,48] of these parameters: for example, at $T=20$ K, VKSLC calculated $\bar{\lambda}_0 = 6.7\times10^{-20}$ m^2, whereas Allison has calculated [47] $\bar{\lambda}_0 = 8.7\times10^{-20}$ m^2 ($\lambda_0 = -\lambda^+/4$ in Allison's notation). Such discrepancies are due to the different, and supposedly better, interatomic potentials used by VKSLC, and because the hyperfine interaction was included in the VKSLC analysis. Of particular importance to the present experiment is the value of the cross section $\bar{\lambda}_1$, as it is the difference $\Omega_{\rm on} - \Omega_{\rm off} \approx -\bar{\lambda}_1/2\bar{\sigma}_2$ that our experiment has measured (see Sec. IV below). Remember that in the semiclassical theory of HI spin exchange, with the atomic nuclei assumed to follow classical paths, one finds $\lambda_1 = 0$ (see discussion in Sec. II A); that is, the HI shift does not depend upon the masing-state population. In the quantum-mechanical VKSLC calculation, howev-

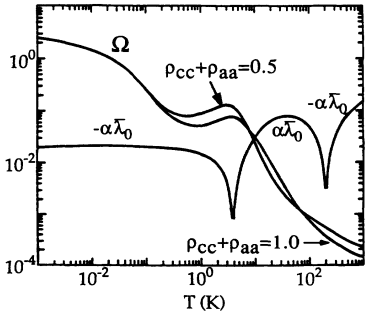

FIG. 3. Dimensionless frequency-shift parameters $\alpha\bar{\lambda}_0$ (for $\alpha = \bar{v}\times10^{9}$ cm^{-3} sec) and Ω (for $\rho_{cc}+\rho_{aa} = 0.5, 1.0$), as functions of temperature. (Figure adapted from Ref. [27].)

er, $|\bar{\lambda}_1| \sim |\bar{\lambda}_2|$ for $0.5 \lesssim T \lesssim 10^4$ K. Thus the result of a "quantum-mechanical" measurement of the HI frequency shift, i.e., one that is sensitive to changes in the massing-state population $(\rho_{cc}+\rho_{aa})$, can be expected to differ significantly from a "semiclassical" measurement such as the experiment of Crampton and Wang [25]. Note also in Fig. 2 that the value of $\bar{\lambda}_1$ changes sign for $T \approx 40$ K. This is due to competing positive and negative partial wave terms in λ_1 [49], and to the specific form of the interatomic potentials and the resulting phase shifts. Changes in these potentials could affect the magnitude and sign of $\bar{\lambda}_1$, and therefore $\Omega_{\rm on}-\Omega_{\rm off}$, as a function of temperature.

Figure 3 displays the VKSLC calculation of Ω, the experimentally accessible HI frequency-shift parameter, as a function of temperature. Ω is plotted for two different massing-state populations $(\rho_{cc}+\rho_{aa})=0.5$ and 1; the difference between these curves illustrates the importance of a proper treatment of rotational symmetry in the H-H spin-exchange problem. Even near room temperature, such a difference should still be observable with a H maser. Measuring this effect is the purpose of the experiment reported here. Also given in Fig. 3 is the well-known DIS spin-exchange frequency-shift term $\alpha\bar{\lambda}_0$ [see Eq. (9)] for a typical H maser value of $\alpha=(10^9$ cm^{-3} sec$)\bar{v}$. As shown in Fig. 3, the HI shift is predicted to become increasingly important as the H temperature is decreased, and to dominate the traditional spin-exchange shift at the operating temperatures of cryogenic H masers ($T<10$ K). This low-temperature dominance is a result of the rotational symmetries of the H-H collision problem, combined with the sharp decline of the spin-exchange relaxation rate with decreasing temperature. Symmetry considerations lead to the functional forms of the HI and direct spin-exchange frequency shifts: $\Omega \sim 1/\gamma_{\rm H}$, thus it is a function of H density; while $\alpha\bar{\lambda}_0$ is independent of the H density (i.e., it is not a function of $\gamma_{\rm H}$). At lower collision energies there are fewer partial waves that contribute to the spin-exchange relaxation. Combined with slower atoms, and hence fewer collisions, the result is that $\gamma_{\rm H}$ drops sharply with temperature for a constant H density (note the calculated values of $\bar{\sigma}_2$ in Fig. 2). This decrease in $\gamma_{\rm H}$ has been measured down to ~ 1 K [50], and is in reasonable agreement with past calculations [48]. Thus Ω is predicted to increase significantly relative to $\alpha\bar{\lambda}_0$, as the H gas temperature is lowered.

In their second paper [27], VKSLC also analyzed the dynamics of the four H hyperfine state populations under typical maser conditions. They developed complete rate equations for the diagonal matrix elements ρ_{vv} $(v=a,b,c,d)$ considering all relaxation processes relevant to normal H maser operation, including H-H spin exchange. They evaluated the inelastic spin-exchange relaxation terms for all allowed channels in the manner outlined above for the elastic terms, except that they used the DIS approximation exclusively. (It was estimated that the inclusion of the hyperfine interaction would only slightly alter these inelastic relaxation results.) For H maser operation near room temperature, as in the present experiment, VKSLC found the following expression for the equilibrium masing-state population in the storage bulb $(\rho_{cc}+\rho_{aa})$:

$$\rho_{cc}+\rho_{aa}=\frac{\gamma_{\rm H}[1-(\rho_{dd}-\rho_{bb})^2]+\gamma_0(\rho_{cc}+\rho_{aa})_{\rm beam}+\gamma_m}{2\gamma_{\rm H}+\gamma_0+2\gamma_m}\ , \tag{11}$$

where

$$\rho_{dd}-\rho_{bb}=\frac{\gamma_0(\rho_{dd}-\rho_{bb})_{\rm beam}}{\gamma_0+\gamma_m}\ .$$

Here $(\rho_{cc}+\rho_{aa})_{\rm beam}$ and $(\rho_{dd}-\rho_{bb})_{\rm beam}$ refer to state populations in the H beam entering the maser storage bulb. Also, γ_0 is the portion of γ_2 due to H escape from the storage bulb and recombination on the bulb surfaces, and γ_m is the atomic-state relaxation rate due to motion through dc magnetic-field gradients present in the bulb. Note that $\rho_{dd}-\rho_{bb}$ is unaffected by spin-exchange relaxation of the hyperfine populations. This is because the total atomic spin magnetic quantum number (m_F) is conserved in a spin-exchange collision. We have used the expressions in Eq. (11) to determine $(\rho_{cc}+\rho_{aa})_{\rm on}$ and $(\rho_{cc}+\rho_{aa})_{\rm off}$ for the interpretation of our measurement of the H HI frequency shift (see Sec. IV below).

III. EXPERIMENTAL APPARATUS AND TECHNIQUES

We have measured hyperfine-induced (HI) spin-exchange frequency shifts in atomic hydrogen (H) near room temperature using a H maser built at the Harvard-Smithsonian Center for Astrophysics (CfA). A schematic of the maser is shown in Fig. 4. (A detailed discussion of H maser principles and technical information is given in the early seminal papers of Kleppner, Goldenberg, Ramsey [23] and Kleppner *et al.* [24] as well as in a recently published two-volume "encyclopedia" of atomic frequency standards, written by Vanier and Audoin [51].) In a CfA H maser, atomic hydrogen is created by dissociating molecular hydrogen (H_2) in a radio frequency (rf) discharge. The H then passes through a hexapole magnet

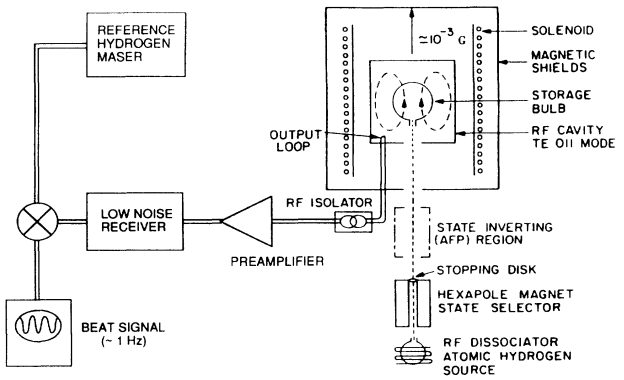

FIG. 4. Schematic representation of a CfA room-temperature hydrogen maser and its associated frequency comparison system.

that focuses the two upper hyperfine states, c and d, along the beam axis and defocuses the lower a and b states. If a single-state selection system is located after the initial hexapole magnet, then the d state atoms are removed from the H beam and the remaining atoms are essentially all in the c state; otherwise the beam consists of approximately equal numbers of c and d state atoms. The focused H beam passes into a cylindrical TE_{011}-mode electromagnetic cavity, resonant at the H c-a hyperfine transition ($\approx$1420 MHz). This H flux produces the population inversion necessary for maser oscillation. The selected atoms are confined in a Teflon-lined spherical quartz storage bulb located at the center of the cavity, where the rf and static magnetic fields are most homogeneous. This confinement increases the interaction time of the atoms with the electromagnetic field in the resonant cavity to about 1 sec, thereby providing the narrow linewidth that is necessary for good frequency stability and measurement precision. Note that the c-a transition is typically used in H masers, as its frequency is independent of the magnitude of the static magnetic field, to first order, at low-field magnitudes (see Fig. 1).

Atoms in the d state do not contribute to maser oscillation, but do participate in spin-exchange collisions that reduce the lifetime of the atoms with a c-a state coherence. The presence of d state atoms also contributes to a magnetic inhomogeneity frequency shift [52,53] (MIS) that can degrade the maser frequency stability. To prevent d state atoms from entering the storage bulb, an adiabatic fast passage (AFP) state inversion mechanism is located between the first hexapole state selection magnet and the resonant cavity [54]. The AFP system consists of a variable-pitch dc solenoid mounted coaxially with the atomic beam, and a rf coil mounted perpendicular to the beam within the dc solenoid. The solenoid creates a longitudinal dc magnetic field that increases in intensity with position along the H beam, while the rf coil superimposes a 5-MHz alternating magnetic field across to the beam. Specifically, the AFP system used in CfA H masers allows the population of masing-state atoms entering the storage bulb to be switched between a value of $\rho_{cc}+\rho_{aa}\approx 1$ with AFP on and $\rho_{cc}+\rho_{aa}\approx 0.5$ with AFP off. This AFP capability is well suited to the present experiment.

Our measurements of HI frequency shifts were performed with a CfA H maser (identification number P27). Changes in the maser frequency were measured relative to an undisturbed reference oscillator, CfA H maser P13. These measurements were made by offsetting the phase-locked receiver frequency synthesizers of the two masers by 1.4 Hz, sending the buffered 1200-MHz output signals from the two masers into a temperature-controlled, double-balanced mixer, and using a computerized, zero-deadtime counter to measure the periods of the resulting beat signals. The counter was set to average the beat period over (roughly) 100 periods, and then to send this information to a computer; the average beat period was then straightforwardly converted to the average beat frequency. Typically, a frequency measurement for a specific condition in maser P27 was conducted by taking a block of 20 to 30 consecutive 100-beat-period averages, and then calculating the mean value of the block beat frequency ($\bar{f}_{\rm beat}$) together with an uncertainty given by the "estimated error of the mean" [55]. The precision of raw $\bar{f}_{\rm beat}$ measurements was limited by the frequency stability of the masers: their characteristic fractional frequency stability is [56] $\sigma_y(\tau)\lesssim 10^{-13}\sqrt{\tau}$ for averaging intervals τ in seconds, on the time scale of the block frequency measurements. [Note that the maser frequency instability decreases as (H flux)$^{-1/2}$ for the low H flux levels used in the present experiment [24].]

The reference H maser (P13) also served as the local frequency reference for a Global Positioning System (GPS) receiver. Common-view GPS measurements coordinated with the National Institute of Standards and Technology (NIST) in Boulder, Colorado, give absolute frequency measurements relative to the unsteered primary time scale NIST(AT1) and to the international time scales UTC (NIST) and UTC. We performed such common-view measurements and established maser P13's long-term frequency drift rate during the performance of the present experiment. The drift rate was found to be about 5 μH/day [57], negligible for the purposes of the present work. This is consistent with the status of maser P13 as a stable, "well-aged" frequency standard not subject to significant internal relaxation phenomena.

To measure the HI shifts we needed to vary $\gamma_{\rm H}$, the H spin-exchange relaxation rate [see Eq. (9)]. $\gamma_{\rm H}$ was altered by changing the H flux into the maser storage bulb, and the value of $\gamma_{\rm H}$ was determined indirectly from the values for γ_2, the atomic dephasing rate, and γ_t, the portion of γ_2 not due to spin-exchange relaxation, yielding $\gamma_{\rm H}=\gamma_2-\gamma_t$. The total relaxation rate γ_2 was measured by offsetting the cavity frequency to four different values over a range of about 4 kHz and observing the resultant pulling of the maser output frequency. Fitting the data to the relation $\Delta\omega_{\rm pull}=\Delta_c\gamma_2$, with $\Delta_c\approx(2Q_c/\omega_0)(\omega_c-\omega_0)$, gives a value for γ_2 with reproducibility $\sim$0.2%. Here, ω_0 is the atomic resonance frequency, while ω_c is the maser cavity's resonance frequency and Q_c is its quality factor. One can have similarly good confidence in measurements of changes in γ_2, whereas the *absolute* value of γ_2 is only known to $\sim$2% because of uncertainty in the absolute values of Q_c and the cavity frequency.

The value of γ_t was determined by measuring γ_2 and the maser radiated power for a number of different H flux levels, and then fitting the data to a well-known relationship derived from standard maser theory [24]. This fit also yields a value for q, a parameter related to important maser operating characteristics [24]:

$$q=K\frac{\gamma_t}{\gamma_0}\frac{1}{(\rho_{cc}+\rho_{aa})_{\rm beam}}\ , \tag{12}$$

where K is a system constant, γ_0 is the portion of γ_2 due to H escape from the maser storage bulb and recombination on the bulb surfaces, and $(\rho_{cc}+\rho_{aa})_{\rm beam}$ is the masing-state population in the H beam entering the storage bulb. Therefore measurements of q for the conditions of AFP on and off serve to determine the effectiveness of the single-state selection system: $q^{\rm off}/q^{\rm on}=(\rho_{cc}+\rho_{aa})^{\rm on}_{\rm beam}/(\rho_{cc}+\rho_{aa})^{\rm off}_{\rm beam}$. Using this

method in the present experiment, we typically found $(\rho_{cc}+\rho_{aa})^{\rm on}_{\rm beam}/(\rho_{cc}+\rho_{aa})^{\rm off}_{\rm beam}=1.82$ to 1.94. In these measurements the maser radiated power is determined from the maser receiver's *IF* level, calibrated independently for the low-level signals ($\sim 10^{-13}$ W) provided by the masing H ensemble. Uncertainties in such absolute power calibrations lead to uncertainties in the absolute values of $\gamma_t \sim 1\%$, and of $q \sim 10\%$ (the uncertainty in the ratio $q^{\rm off}/q^{\rm on}$ is only $\sim 3\%$, however).

The masing atoms are confined inside the resonant cavity within a spherical storage bulb (7 in. diameter) made of thin fused silica. The storage bulb has a small, collimated aperture through which the H both enters and departs, after a storage time of about 1 sec. The bulb is coated internally with Teflon FEP-120 [58]. Because of the benign properties of Teflon, only a moderate amount of $H+H \rightarrow H_2$ recombination takes place on the bulb walls, even though each atom has a wall collision rate $\sim 10^4$/sec. There is, however, a significant frequency shift associated with these wall collisions.

During wall collisions, very brief deformations of the H electron cloud occur as part of transient van der Waals interactions. Such deformations cause phase changes in the hyperfine interaction. The average phase shift per collision multiplied by the collision rate yields the wall frequency shift. These shifts have been found to depend on the nature and texture of the particular Teflon coating in a specific H maser, as well as on the temperature of the atom/wall system. Good temperature control can keep the wall shift quite steady, such that H maser frequency stability is not limited by this effect. Nevertheless, the typical wall shift is quite large (~ -30 mHz for a 17.8-cm-diameter storage bulb) relative to typical H maser measurement precision ($< 10\ \mu$Hz). The irreproducibility of the wall shift from maser to maser, and the large wall shift magnitude, limit the *accuracy* of H maser frequency standards.

In CfA H masers the contribution of wall relaxation (γ_w) to the total dephasing rate (γ_2) has been found to vary with time. Typically, γ_w is a small fraction of γ_2 for a new Teflon wall coating ($\gamma_2 \sim 1\ {\rm sec}^{-1}$ at low H flux levels). Within the first few months of exposure to vacuum and to H, however, γ_w steadily increases—usually by about 0.3 $\rm sec^{-1}$ for a successful coating—before slowly leveling off after a year or more. This Teflon aging in H masers is still not well understood, although it may be due to a slow, chemical reaction between the H and the fluorine-dominated end groups of the Teflon polymer material [59]. Sometimes, the Teflon aging does not stabilize; instead, the wall degradation accelerates after a few months, the maser eventually ceases to oscillate, and the storage bulb must be removed and recoated with Teflon. This occurred in the maser used in the present experiment (CfA maser P27) after the completion of the data taking reported here (see discussion in Sec. IV B). Note that there has been no evidence that this type of Teflon aging is accompanied by a significant change in the wall frequency shift on the time scale relevant to the present experiment (about one day). This is consistent with the model of wall relaxation being due to atom loss processes, namely, $H+H \rightarrow H_2$ recombination and H plus Teflon chemical reaction.

The maser rf cavity is a TE_{011}-mode resonator tuned very close to the H hyperfine transition frequency (≈ 1420 MHz). Atoms that enter the cavity storage bulb are confined to a volume where the oscillating rf magnetic field is approximately uniform and oriented parallel to a weak, spatially homogeneous static magnetic field. This static field is produced by a main solenoid and two trim coils mounted on the outside of the vacuum bell jar that surrounds the cavity. The currents for the three solenoids are supplied by a voltage regulator configured as three constant current sources by three adjustable current-setting resistors. This setup allows control to approximately 1 μG in the static field (B_0), with the maser typically operated with $B_0 \approx 0.5$ mG. Surrounding the solenoids are four layers of nested, cylindrical magnetic shields (with end caps) to isolate the maser cavity from the magnetic field of the earth and other external sources. Typical CfA H maser shields have a net shielding factor $\Delta H_{\rm external}/\Delta H_{\rm internal} \gtrsim 5\times 10^4$, and thus attenuate the earth's field (~ 0.5 G) to an insignificant level ($\sim 10\ \mu$G). There is also a few-turn coil wrapped on two sides of the cylindrical vacuum bell jar that surrounds the resonant cavity. This allows a transverse, audio frequency magnetic field to be applied to the atoms in the maser storage bulb, in order to induce $\Delta F=0$ Zeeman frequency transitions (*d-c* and *c-b*). This Zeeman frequency can then be determined by the resultant decrease in the maser output power when the applied signal is resonant with the $\Delta F=0$ transitions. From the measured Zeeman frequency value one can determine the strength of the spatially averaged static magnetic field in the storage bulb, and hence calculate the *second-order* Zeeman shift to the *c-a* transition. For typical low-field operation ($B_0 \approx 0.5$ mG), we could measure the $\Delta F=0$ Zeeman frequency (≈ 700 Hz) to about 0.05 Hz; this allows a determination of the second-order *c-a* frequency shift to approximately 0.1 μHz.

In the H maser used in the present experiment (CfA maser P27) the cylindrical cavity body and the two cavity end caps are made of Zerodur [60], a glass-ceramic dielectric material characterized by: (i) low thermal expansion; (ii) mechanical stiffness; (iii) long-term dimensional stability; and (iv) total absence of para- and ferromagnetism. The Zerodur cavity superstructure is coated internally with a thin layer of silver to produce an electromagnetic resonant cavity with the necessary Q. The joints between the cavity cylinder and the end caps are optically smooth when contacted, and are maintained under a force ~ 2000 N. CfA H masers typically exhibit upward drifts in their cavity frequencies due to a settling of cavity materials and joints [61]. This cavity frequency drift in turn causes the observed maser output frequency to drift upward with time. The settling of the cavity dimensions typically has a time constant of several months; hence the maser frequency drift is quite linear on the time scale of hours to a few days that is relevant to the present experiment.

In CfA H masers the cavity frequency can be controllably varied in steps of approximately 0.1 Hz, over a range of roughly 10 kHz, by a voltage-controlled (varactor)

diode that is inductively coupled to the cavity. A reverse voltage applied to the diode varies its capacitance and thus the reactance coupled to the cavity; this changes the cavity resonance frequency. The diode's pulling of the maser frequency is kept constant to better than 1 μHz with the use of an extremely stable bias-voltage supply.

The cavity frequency drift was found to be quite large for the (recently constructed) maser P27, resulting in a maser output frequency drift ~ 100 μHz/day. This proved to be a significant correction to the raw frequency measurement data, as discussed in Sec. IV below. We observed the cavity frequency drift indirectly by periodically measuring the "flux-tuned" varactor diode voltage over a three-month period that contained all data runs for the present experiment. [Flux-tuning the cavity leaves the maser output frequency largely insensitive to changes in the H flux: using the notation of Eq. (9) this amounts to setting $\Delta_c \approx -\alpha\bar{\lambda}_0$, ignoring the much smaller HI shift.] The diode voltage can be accurately related to a pulling of the cavity frequency, with approximately 1Hz/mV; hence the cavity frequency drift is well characterized by monitoring changes in this diode voltage (see Fig. 5). P27's cavity frequency drift was much larger than that of previous CfA H masers at similar time intervals after assembly. This is consistent with the use of Zerodur for the cavity body, in contrast to the use of Cer-Vit [62] in previous H masers built at CfA. (Most of these masers are currently in use at radio observatories and timekeeping stations throughout the world.) Cer-Vit is also an inert glass-ceramic, but with properties superior to Zerodur for use in maser cavities. Unfortunately, Cer-Vit became commercially unavailable in the early 1980s, and remaining stock supplies have recently been exhausted.

Temperature variations can significantly affect the maser frequency through changes in the storage bulb dielectric coefficient and the cavity dimensions. To achieve frequency stability of 1×10^{-15} (≈ 1 μHz absolute frequency precision), the cavity and bulb temperature must be held constant to roughly 10^{-4} K. This is accomplished in CfA H masers by employing multiple levels of thermal guard ovens, each with an independent temperature control circuit. The net thermal isolation of the vacuum bell jar that surrounds the resonant cavity from changes in the external room temperature was measured to be $\sim 10^{-5}$, for a H maser of the type used in the present experiment. Thus a 1-K change in ambient temperature will change the bell jar temperature by only 10^{-5} K; this would cause an insignificant maser frequency excursion (<1 μHz). All equipment used in the present experiment was maintained in a room that was temperature regulated to ± 0.5 K. Note that the thermal links between the bell jar, the resonant cavity, and the storage bulb are purposefully made weak. This results in a long thermal time constant (~ 7 h) for the maser frequency to respond to changes in the external temperature, further reducing the maser sensitivity to short-term temperature excursions. For maser P27 the control temperature for the resonant cavity and storage bulb, and hence the masing H ensemble as well, was 323 K.

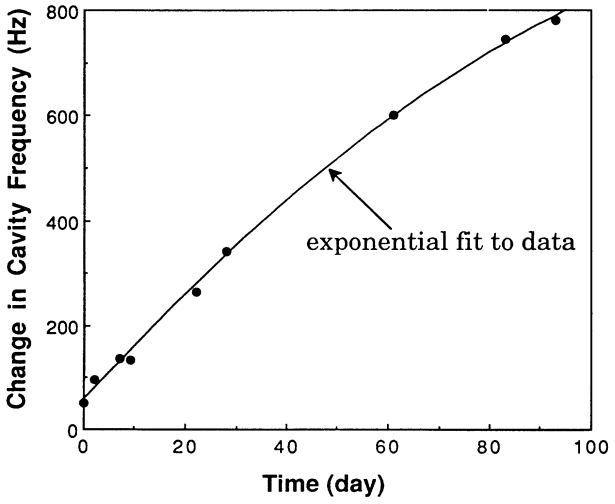

FIG. 5. Measured change of the resonant cavity frequency of hydrogen maser P27 over a period of a few months.

Transient fluctuations in the maser cabinet air temperature can cause phase variations in the coaxial cables and electronic components used in the maser. This can lead to a transient deviation in the observed maser frequency. Tests have been performed on a maser similar to the one used in the present experiment. It was found that the fractional frequency deviation is related to the rate of change of the cabinet air temperature by $\Delta f/f \sim (5\times10^{-13})dT/dt$ (time in seconds). In steady state the cabinet air temperature is controlled to at least ± 0.050 K, over a period ~ 30 min. This implies only insignificant maser frequency deviations (<1 μHz). However, when changing the level of H flux, or turning the AFP system on or off, the resulting large cabinet air temperature transient could cause observed frequency deviations ~ 50 μH. For changes in the H flux level this temperature transient was due to altering the amount of heat being applied to the palladium valve that controls the flow of H_2 to the dissociator. For changes in the AFP state it was due to connecting or disconnecting the 5-MHz current supply (internal to the maser) to the AFP system's transverse rf coil, as there is a large amount of heat dissipated by the rf system. Thus after every change in the H flux or the AFP state we allowed the maser temperature control systems to reestablish a steady-state condition, and any phase and frequency deviations to die away, before proceeding with our measurements. Typically, such reequilibration processes took from 30 to 60 minutes.

IV. EXPERIMENTAL RESULTS

We have measured the difference between the atomic-hydrogen (H) HI spin-exchange frequency shift for AFP on and AFP off, using CfA H maser P27. These two AFP conditions affect the population of the two H masing states (the c and a states) as follows: $(\rho_{cc}+\rho_{aa})\approx 1$ for AFP on, and $(\rho_{cc}+\rho_{aa})\approx 0.5$ for AFP off. The magnitude of the HI shift is characterized by the parameter Ω [see Eq. (10)] and is predicted to depend upon the masing-state population by the quantum-mechanical

theory of VKSLC [26,27], but not by the semiclassical theory due to CW [25]. Thus our measurement of $\Omega_{on}-\Omega_{off}$ provides important new information about quantum-mechanical HI effects in atomic spin-exchange collisions.

We have measured HI shifts for two distinct yet complementary modes of H maser operation: at a "low" level of static magnetic field (≈ 0.5 mG), and at a 'high" magnetic field (≈ 30 mG). Operating a H maser at low field has the advantage of superior performance as a frequency standard. In this condition the short-term frequency stability (approximately seconds to minutes) is very good. But most importantly, the medium-term stability (approximately minutes to hours) is also good because the *c-a* transition frequency at low fields is quite insensitive to changes in the magnetic field, whether due to variations in the current supplying the maser solenoids or due to external field fluctuations. Therefore at low field there are few problems with Zeeman-induced frequency drift on the time scale of a data-taking run (about one day); hence one can directly monitor the linear, cavity-induced maser frequency drift for some period before and after data taking and then reliably correct for this effect. Additional advantages to low-field operation include the option of taking data at any time, not just in the middle of the night when the external magnetic field environment is quiet (see discussion below for the high-field case); also, the ability to precisely measure the Zeeman splitting of the *d* and *b* hyperfine states from the *c* state, and from this to determine precisely the second-order Zeeman splitting of the *c-a* maser transition. The singular disadvantage of low-field operation is the presence of the magnetic inhomogeneity shift (MIS), which can masquerade as the HI frequency shift (see discussion below). As a solution to this systematic problem at low fields, we measured the MIS with a technique first developed by Reinhardt and Peters [63], and then corrected our HI shift measurements to yield values for $\Omega_{on}-\Omega_{off}$.

The singular benefit of making HI shift measurements at high field is the absence of the MIS. It effectively disappears at high magnetic fields, where the $\Delta F=0$ Zeeman transition frequencies are large relative to the rate that H atoms in the storage bulb bounce back and forth through whatever small magnetic gradients are present. The most significant disadvantage of high-field operation is the greatly increased sensitivity of the maser frequency to field fluctuations. The second-order Zeeman shift to the *c-a* transition frequency is given by $\Delta f_{maser} \approx 2750\langle B_0^2\rangle_{bulb}$, where f_{maser} is in units of hertz and B_0 is in gauss, and the brackets imply a spatial average over the storage bulb volume. Thus a 0.1-μG field variation at high field causes a large 16-μHz frequency shift, while at low field the same variation would change the maser frequency by less than 1 μHz. Because of this sensitivity to field fluctuations the high-field H maser frequency is generally less stable in the medium term, making it much more difficult to perform a complete high-field HI shift measurement. For example, reliable high-field data could only be taken in the early morning hours when the external magnetic field "noise" was low. This noise was largely due to the nearby subway, as well as to buses powered by overhead electrical lines, and was measured with a flux-gate magnetometer to have an amplitude ~ 5 mG. With a magnetic shielding factor $\sim 5\times 10^4$, this implies significant maser frequency deviations ~ 16 μHz.

A second major technical problem with the high-field HI measurement was the control of the maser's internally supplied static magnetic field. The voltage regulator used to supply the maser solenoid currents (see discussion in Sec. III) is weakly sensitive to temperature. The total range of the maser cabinet's internal air temperature is only ~ 100 mK, during changes of low to high H flux or changes in the AFP condition; however, this is sufficient to cause small changes in the solenoid currents and hence large second-order Zeeman shifts in the maser frequency at high field. This problem was solved by supplying the solenoids for the H maser under test (CfA maser P27) with currents from a separate, undisturbed maser (CfA maser P28).

Two successful low-field data-taking runs and one high-field run were completed in the present experiment. (Unfortunately, maser P28 was only available for a limited period of time [64], and so additional high-field data-taking runs could not be performed.) In the following subsections the measurement procedures, data, and methods of data analysis are presented for the low-field and then for the high-field work. As will be seen below, the results for $\Omega_{on}-\Omega_{off}$ from these two modes of operation are found to be comparable, and to indicate a dependence of the H HI shift on the atomic hyperfine state populations. However, the measured magnitude and sign of $\Omega_{on}-\Omega_{off}$ are found to disagree with the prediction of the quantum-mechanical VKSLC theory.

A. Low-field results

The experimental procedure we used at low field follows directly from the expression for the maser output frequency developed by VKSLC [see Eqs. (9) and (10) above]:

$$\omega-\omega_0=[\Delta_c+\alpha\bar{\lambda}_0]\gamma_2-(\Omega-\varepsilon_m)\gamma_H\ , \tag{13}$$

where the term $\varepsilon_m\gamma_H$ has been added to account for the MIS [25]. One can measure the maser frequency as a function of γ_2, by varying the H beam flux, and determine the slope (m) of this relationship. The difference between the slopes for the conditions of AFP off and on will then yield

$$m_{off}-m_{on}=(\varepsilon_m^{off}-\varepsilon_m^{on})+(\Omega_{on}-\Omega_{off})\ . \tag{14}$$

Therefore with an independent measurement of $\varepsilon_m^{off}-\varepsilon_m^{on}$ the HI shift parameter difference $\Omega_{on}-\Omega_{off}$ can be determined.

In our low-field measurements the specific experimental procedure was as follows.

(1) Monitor the maser frequency drift in a steady-state condition for a day or more before beginning the data-taking run. This allows the effect of the cavity frequency drift to be characterized and removed from the raw data (see discussion in Sec. III).

(2) Begin at a low H flux value with AFP on. Measure the maser frequency and γ_2. (The measurement pro-

cedures are outlined in Sec. III.)

(3) Turn the AFP off (disconnect the rf supply from the AFP coil) and allow the maser cabinet temperature control system to reequilibrate. Then measure the maser frequency and γ_2.

(4) Increase the H flux, allow temperatures to reequilibrate, and repeat the measurements for AFP off and then for AFP on.

(5) Repeat this process for several H flux levels. The total range of H flux should not be too large so as to significantly alter the masing-state populations by spin-exchange relaxation [see Eq. (11)].

(6) At high H flux measure the MIS, both for AFP on and off, using the Reinhardt-Peters method [63] (discussed below).

(7) Return to low H flux and AFP on and resume the monitoring of the long-term maser frequency drift.

The MIS arises from second-order processes that couple the c-a coherence to the $F=1$ "stretch" states (d and b) via atomic motion through dc and rf magnetic field gradients in the maser storage bulb [52,53]. The coupling to the d state pulls the maser frequency higher, while the b state coupling pulls it lower. Since such second-order processes depend on the occupancies of the relevant states, one finds that the net MIS is a function of $(\rho_{dd}-\rho_{cc})+(\rho_{cc}-\rho_{bb})$; that is

$$\varepsilon_m = K(\rho_{dd}-\rho_{bb}) , \tag{15}$$

where the parameter ε_m characterizes the size of the MIS and K is a function of the distribution of static and rf field gradients in the maser bulb. The analysis of Crampton and Wang [52,53] indicates that the magnitudes of the two processes that contribute the most to the MIS should scale as γ_m and as $(\gamma_m)^{1/2}$ (where γ_m is the atomic-state relaxation rate due to motion through dc magnetic gradients). Note also that with perfect AFP, $(\rho_{dd}-\rho_{bb})=0$ and hence there is no MIS.

The Reinhardt-Peters method for determining the MIS consists of measurably inverting the "atomic magnetization" $(\rho_{dd}-\rho_{bb})$, while leaving all other relevant parameters undisturbed, and then observing the resultant change in the maser frequency. Once γ_H is known from measurements of γ_2 and γ_t (see discussion in Sec. III), ε_m is found from the following:

$$\varepsilon_m = (\omega_{normal}-\omega_{\text{inverted}}) \times \left[1-\frac{(\rho_{dd}-\rho_{bb})_{\text{inverted}}}{(\rho_{dd}-\rho_{bb})_{\text{normal}}}\right]^{-1} \gamma_H^{-1} . \tag{16}$$

A relative measure of $(\rho_{dd}-\rho_{bb})$ is provided with a double resonance technique due to Andresen [65]. A transverse, audio frequency magnetic field is applied to the H atoms in the maser near their Zeeman (c-d and c-b transition) frequency. As this field is slowly swept through the Zeeman resonance the maser output frequency (at the c-a transition) exhibits a large (~ 0.01 Hz), antisymmetric excursion. For low transverse field powers the magnitude of the maser frequency deviation is proportional to $(\rho_{dd}-\rho_{bb})$.

In our work we achieved near perfect inversion of $(\rho_{dd}-\rho_{bb})$ merely by reversing the direction of the static field (B_0), provided by the maser cavity solenoids, relative to the direction of the field in the beam tube outside the nested magnetic shields. This was easily accomplished by reversing the sense of the currents supplied to the solenoids. After making minor adjustments to the top-end solenoid, located near the joint of the beam tube and the cavity, we consistently found no significant difference between the γ_2's measured for the "normal" and "inverted" conditions. Thus we had confidence that the magnitude of the field gradient parameter K [see Eq. (15)] was not significantly affected by the field inversion. Also, using the Andresen technique with AFP off, we consistently found $(\rho_{dd}-\rho_{bb})_{\text{inverted}}/(\rho_{dd}-\rho_{bb})_{\text{normal}} \approx -0.95$ to -1.05, good evidence that near perfect state inversion had taken place. A typical measurement of this inversion is shown in Fig. 6. Using the Andresen technique with AFP on we found much smaller maser frequency excursions (see Fig. 7), generally a factor of 20 less than with AFP off, good evidence that the AFP system was providing near perfect masing-state selection.

Following the experimental procedure outlined above, we performed two complete HI measurements at low field. We shall refer to these data runs as LF1 and LF2. The runs were completed in a four-day period that included time for monitoring the maser frequency drift before the first run (LF1), between the runs, and after LF2. The two runs had opposite designations for normal and inverted static magnetic fields: the frequency versus γ_2 data for LF1 were taken with "$-$" fields, while "$+$" fields were used to measure the MIS; for LF2 the frequency versus γ_2 data were taken with $+$ fields, while the MIS measurement involved $-$ fields. For both runs the raw frequency data were corrected for the cavity frequency drift and for small, second-order Zeeman frequency shifts. These corrected results are displayed in Figs. 8 (for LF1) and 9 (LF2).

The frequency data shown in Figs. 8 and 9 include all

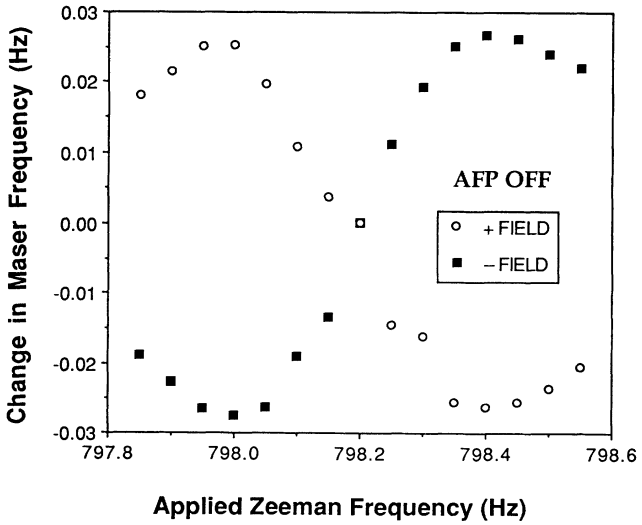

FIG. 6. Typical measured comparison of the Andreson effect for "normal" and "inverted" static magnetic fields. The AFP off condition was used for both field orientations.

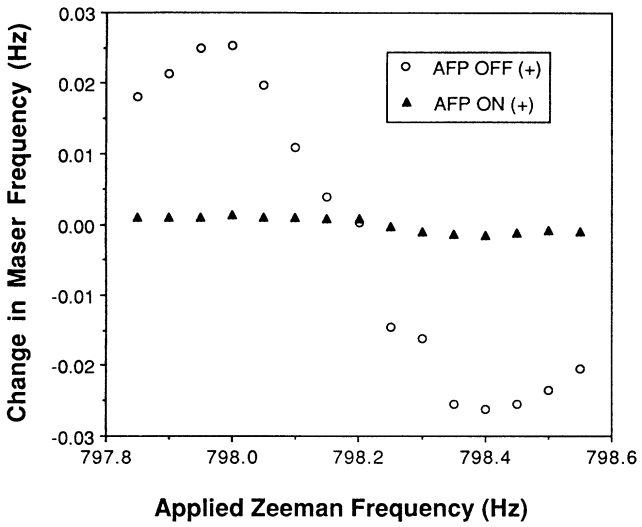

FIG. 7. Typical measured comparison of the Andresen effect for the AFP off and AFP on conditions.

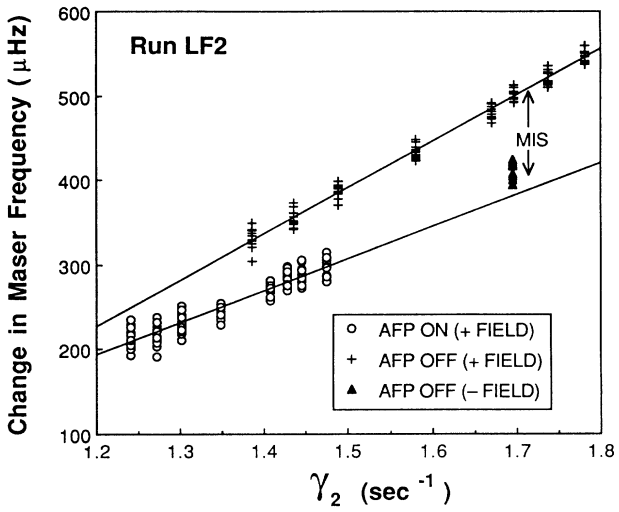

FIG. 9. Hydrogen maser frequency vs linewidth data for run LF2. Note that the sense of the "normal" and "inverted" magnetic fields has been reversed from run LF1.

the individual measurements derived from the canonical 100-beat-period averages (see discussion in Sec. III). When performing a linear regression analysis on these data, however, we used the mean values ($\bar{f}_{\rm beat}$) of the blocks of frequency measurements, one for each level of H flux (each γ_2 value). Note that the uncertainty in $\bar{f}_{\rm beat}$, initially taken as the "estimated error of the mean" [55] of the raw data, was adjusted to account for the uncertainty in the correction for cavity frequency drift (typically a small adjustment). Examining the trends of the frequency versus γ_2 data, one sees a clear distinction between the differences in slope $m_{\rm off}-m_{\rm on}$ for LF1 and for LF2. This is simply the effect of reversing the sign of the

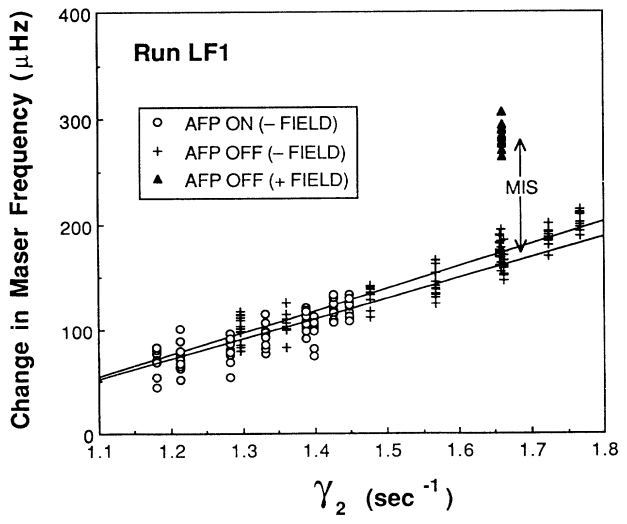

FIG. 8. Hydrogen maser frequency vs linewidth data for run LF1. Measurements for AFP on and off are shown, as well as the AFP off data with "inverted" magnetic fields used to determine the MIS.

MIS. Using the Reinhardt-Peters method we found $\varepsilon_m^{\rm off}=-5.51\ (0.34)\times10^{-4}$ and $\varepsilon_m^{\rm on}=-0.06\ (0.64)\times10^{-4}$ for LF1, and $\varepsilon_m^{\rm off}=5.75\ (0.34)\times10^{-4}$ and $\varepsilon_m^{\rm on}=0.07\ (0.73)\times10^{-4}$ for LF2. Combining this information with the fitted values for $m_{\rm off}-m_{\rm on}$, we determined the low-field HI shift parameters [see Eq. (14)] to be

$$\Omega_{\rm on}-\Omega_{\rm off}=\begin{cases}5.26(1.79)\times10^{-4}, & \text{LF1} \quad (17)\\ 3.80(1.49)\times10^{-4}, & \text{LF2}\ . \quad (18)\end{cases}$$

Note the reasonable agreement between the values for $\Omega_{\rm on}-\Omega_{\rm off}$ determined by the two low-field runs. For both LF1 and LF2, the error in $\Omega_{\rm on}-\Omega_{\rm off}$ is a 1-standard-deviation uncertainty that includes the statistical uncertainties from $m_{\rm off}-m_{\rm on}$ (1.63×10^{-4} for LF1 and 1.26×10^{-4} for LF2) and $\varepsilon_m^{\rm off}-\varepsilon_m^{\rm on}$ (0.71×10^{-4} for LF1 and 0.76×10^{-4} for LF2), as well as an estimate of the systematic uncertainty in $\gamma_{\rm H}$ as it affects the fit (0.20×10^{-4} for LF1 and 0.27×10^{-4} for LF2), all combined in quadrature. In the fits described above (as well as the fits to the high-field results, discussed in Sec. IV B) the χ^2 per degree of freedom (χ_ν^2) was typically ~1. For fits with $\chi_\nu^2>1$ the associated parameter variances were corrected by multiplying by χ_ν^2.

We calculated the LF1 and LF2 values for $(\rho_{cc}+\rho_{aa})_{\rm on}$ and $(\rho_{cc}+\rho_{aa})_{\rm off}$ using the expressions in Eq. (1) and our measurements of γ_2, γ_t, $q^{\rm off}/q^{\rm on}$, etc. The remnant magnetic gradient relaxation rate ($\gamma_m\approx0.11\ \text{sec}^{-1}$) was determined by comparing the values for γ_t at low field and at high field (where $\gamma_m=0$). Taking $(\rho_{cc}+\rho_{aa})_{\rm beam}^{\rm off}=(\rho_{dd}-\rho_{bb})_{\rm beam}^{\rm off}=0.5$, we found $(\rho_{cc}+\rho_{aa})_{\rm on}=0.72$ to 0.80 and $(\rho_{cc}+\rho_{aa})_{\rm off}=0.45$ to 0.47, for high to low H flux as used in the low-field runs.

B. High-field results

The high-field data-taking run was performed roughly one month after the two low-field data-taking runs. We

shall refer to the high-field run as HF. Operating the test maser (P27) at high fields (≈ 30 mG) there was no MIS. This was verified by applying a significant magnetic field gradient to the maser, in addition to the 30-mG static field, and observing that the value of γ_2 was unchanged. Thus $\gamma_m = 0$ at high field and so $\varepsilon_m = 0$ [53]. Therefore from Eq. (14) one sees that a high-field measurement of the maser frequency as a function of γ_2 should directly determine $\Omega_{on} - \Omega_{off}$. It was necessary, however, to make an additional, systematic correction to our measurement of $m_{off} - m_{on}$ to account for the accelerated degradation of the Teflon wall coating suffered by maser P27 during the high-field run (see discussion in Sec. III). The wall relaxation rate γ_w was not perfectly constant during the run (total change ≈ 0.03 sec^{-1}); hence the measured change in γ_2 did not exactly equal the change in γ_H, as assumed in deriving Eq. (14) above. Also, any change in γ_w would pull the maser frequency, since the cavity was not perfectly "tuned" ($\Delta_c \neq -\alpha\bar{\lambda}_0$), and this pulling could be slightly different for AFP on and off. Note that this wall degradation correction to $\Omega_{on} - \Omega_{off}$ was relatively small for run HF ($\approx 10\%$) and negligible for the earlier low-field runs ($\approx 3\%$), given the overall precision of this experiment and the magnitude of the disagreement with theory.

The specific experimental procedure employed in the high-field measurement was very similar to that used at low field (and outlined in Sec. IV A), except for the following points.

(1) There was no need to measure the insignificant MIS.

(2) Maser P28 supplied the high-field current for itself and for the test maser P27, in a parallel configuration. P28's frequency was monitored throughout the run and served as a "witness" to the static field stability. Any significant frequency excursions away from a linear, cavity-induced frequency drift, that were shared by both P27 and P28, served as criteria to reject the high-field data. Given the typical short-term H maser frequency stability at high field, however, this witness mechanism was only sensitive to systematic frequency deviations $\gtrsim 30\ \mu$Hz.

(3) It was not possible to measure the Zeeman frequencies to sufficient accuracy to correct the HF frequency data for second-order Zeeman shifts smaller than about 100 μHz. (Note that at high field the *d-c* and *c-b* transitions are split by roughly 3 Hz).

(4) The active, data-taking part of the run was confined to the early morning hours, when the external magnetic field environment was sufficiently quiet.

The raw HF frequency versus γ_2 data were corrected for the cavity frequency drift. These corrected results are shown in Fig. 10. In contrast to the presentation in Figs. 8 and 9 of all the individual frequency measurements for runs LF1 and LF2, Fig. 10 displays the mean values of the HF frequency data at each H flux level. (The error bars are given by the estimated error of the mean [55] for each block of frequency measurements.) Note that only five AFP off and six AFP on H flux levels were used in the HF run; this was because of the shortness of the late night "measurement window." Including all the data shown in Fig. 10, fitting for the slopes of the AFP on and off frequency versus γ_2 trends, and correcting for the wall degradation during the run, we determined the high-field HI shift parameter difference:

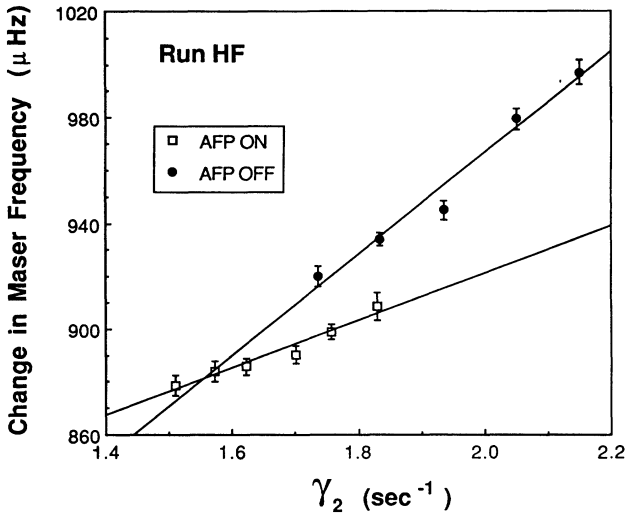

FIG. 10. Hydrogen maser frequency vs linewidth data for run HF. The weighted means of the measured frequencies at each hydrogen flux level are shown here, with the error bars given by the "estimated error of the mean." This is in contrast to Figs. 8 and 9, where all the frequency data for runs LF1 and LF2 are displayed.

$$\Omega_{on} - \Omega_{off} = 7.33(1.61) \times 10^{-4}, \quad \text{HF (all data)}, \tag{19}$$

where the error in $\Omega_{on} - \Omega_{off}$ ($= 1.61 \times 10^{-4}$) is a 1-standard-deviation uncertainty that includes the statistical uncertainty in $m_{off} - m_{on}$ ($= 1.58 \times 10^{-4}$), and an estimate of the systematic uncertainty in $\Delta\gamma_H$ as it affects the fit ($= 0.31 \times 10^{-4}$), combined in quadrature.

One can see in Fig. 10 similar small deviations away from a linear frequency versus γ_2 trend, for both AFP on and AFP off: a possible slight depression of the measured frequencies for the intermediate γ_2 values. This effect may have been purely random, or it may have been a small systematic excursion in the net magnetic field. Excluding the frequency data for the "middle" AFP off H flux value ($\gamma_2 \approx 1.94$ sec^{-1}) and the "fourth" AFP on H flux value ($\gamma_2 \approx 1.7$ sec^{-1}), and redoing the data analysis, we found

$$\Omega_{on} - \Omega_{off} = 7.40(1.24) \times 10^{-4}, \quad \text{HF (edited data)}. \tag{20}$$

Thus the possible small magnetic field excursion does not significantly affect the high-field determination of $\Omega_{on} - \Omega_{off}$.

We calculated the HF values for $(\rho_{cc} + \rho_{aa})_{on}$ and $(\rho_{cc} + \rho_{aa})_{off}$ using the expressions in Eq. (1) and our measurements of γ_2, γ_t, q^{off}/q^{on}, etc. Taking $(\rho_{cc} + \rho_{aa})^{off}_{beam} = (\rho_{dd} - \rho_{bb})^{off}_{beam} = 0.5$, we found $(\rho_{cc} + \rho_{aa})_{on} = 0.78$ to

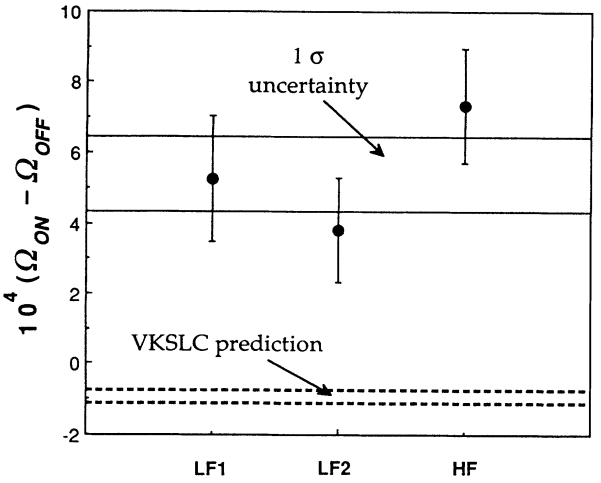

FIG. 11. Experimentally determined values of $\Omega_{on}-\Omega_{off}$ for the three runs reported in the present work. The one-standard-deviation limit on the weighted mean of these values is displayed. Also shown is the theoretical prediction of VKSLC for $\Omega_{on}-\Omega_{off}$, over the range of $(\rho_{cc}+\rho_{aa})$ values used in this experiment.

0.88 and $(\rho_{cc}+\rho_{aa})_{off}=0.44$ to 0.47, for high to low H flux as used in the HF run.

The low- and high-field results for $\Omega_{on}-\Omega_{off}$ are comparable [see Eqs. (17)–(20)]. Assuming that this agreement supports the veracity of both the low- and high-field measurement techniques, one can take the weighted mean of the LF1, LF2, and HF values for $\Omega_{on}-\Omega_{off}$ [using Eq. (19) for HF]:

$$\Omega_{on}-\Omega_{off}=5.38(1.06)\times10^{-4}, \text{ weighted mean} . \quad (21)$$

This weighted mean, as well as the values from the individual data runs, significantly disagree with the VKSLC prediction [66] of $\Omega_{on}-\Omega_{off}=-0.76\times10^{-4}$ to -1.12×10^{-4} at the H temperature used in our experiment (323 K), and for the relevant range of state population values: $(\rho_{cc}+\rho_{aa})_{on}=0.72$ to 0.88 and $(\rho_{cc}+\rho_{aa})_{off}=0.44$ to 0.47. Figure 11 shows the results of the three data-taking runs, the 1-standard-deviation confidence limits on the weighted mean, and the range of VKSLC predictions for $\Omega_{on}-\Omega_{off}$.

V. DISCUSSION

In this section we review our experimental results, compare them to the relevant theoretical calculations, and suggest avenues for future research. We have used atomic hydrogen (H) masers and measured a dependence of the H hyperfine-induced (HI) spin-exchange frequency shift on the atomic hyperfine populations. This measured dependence agrees qualitatively with the quantum-mechanical theory of H-H spin-exchange collisions due to Verhaar, Koelman, Stoof, Luiten, and Crampton and supports the basic symmetry arguments they have used to treat this problem. However, both the magnitude and the sign of our measured value for the H HI shift parameter difference $\Omega_{on}-\Omega_{off}$ disagree with the VKSLC numerical calculation. Next, we examine some possible reasons for this discrepancy.

One possibility is that better interatomic potentials are needed, and hence that VKSLC's numerical calculations for the HI shift parameter difference $\Omega_{on}-\Omega_{off}$ are incorrect. Examining the VKSLC expression for Ω [Eq. (10)] and their calculation of the magnitudes of the relevant cross sections (Fig. 2), one sees that the present HI measurement is sensitive to the frequency-shift cross section λ_1, but not to λ_2: $\Omega_{on}-\Omega_{off}\approx-\bar{\lambda}_1/2\bar{\sigma}_2$. This measurement is the first experimental determination of such a "quantum-mechanical" HI effect. (In the semiclassical theory $\lambda_1=0$, as discussed in Sec. II A.) VKSLC found $\bar{\lambda}_1$ to vary significantly with H gas temperature, and to change sign for $T=T_x\approx40$ K (see Fig. 2). This is because of the competing positive and negative partial wave terms in λ_1, and because of the specific form of the H-H triplet and singlet potentials used in the numerical calculation, which influence the resulting partial wave phase shifts. Note that changes in these potentials could shift the "crossover" temperature T_x higher or lower, and thereby change the magnitude and sign of $\bar{\lambda}_1$, and thus $\Omega_{on}-\Omega_{off}$, as a function of temperature. Using our measured value for $\Omega_{on}-\Omega_{off}$ [Eq. (21)] and the well-known value for the relaxation cross section ($\bar{\sigma}_2\approx1.16\times10^{-19}$ m^2) [21,22], we determine $\bar{\lambda}_1|_{\text{experiment}}\approx-1.8\times10^{-22}$ m^2 for $T=323$ K. This contrasts in both sign and magnitude with the VKSLC calculation of $\bar{\lambda}_1\approx3.0\times10^{-23}$ m^2 at this temperature ($T>T_x$), but is in rough agreement with their $\bar{\lambda}_1$ value for $T\sim1$ or 10 K ($T<T_x$). Thus it is possible that improved interatomic potentials could increase T_x sufficiently to eliminate the discrepancy between theory and experiment.

In addition, there may be other problems with the VKSLC calculation of $\Omega_{on}-\Omega_{off}$. Perhaps there is a breakdown in the high-collision-energy (first-order) approximation used to calculate the thermally averaged cross section $\bar{\lambda}_1$ near room temperature (see discussion in Sec. II B). This seems unlikely, however, given the careful comparisons that VKSLC made between the first-order and "exact" coupled-channel calculations. Or perhaps there is some overlooked physics in the H maser system that mimics the HI frequency shift. Such a process would need to have the same functional dependence as the HI shift upon the collisional relaxation rate γ_H and the masing-state population $\rho_{cc}+\rho_{aa}$ [see Eqs. (10) and (13)], because the data from the present experiment are well described by the current formalism (albeit with the parameter $\bar{\lambda}_1$ assuming a value different from that calculated by VKSLC). Also, any new physics would probably have to be unrelated to magnetic effects, such as the magnetic inhomogeneity shift [52,53], since our measured high- and low-field results are in reasonable agreement. Further investigation of all the above theoretical questions is probably warranted.

Of course, it is possible that systematic errors in the present experiment may have led to the disagreement with the VKSLC theory. We next discuss our considerations of such systematic experimental error. One possibility is that there was a wall frequency shift that depend-

ed on the H density in the maser storage bulb (see discussion of the wall shift in Sec. III). To account for the discrepancy between experiment and theory, this wall shift would need to be nonlinear in the H density (i.e., in γ_H), because a linear effect would affect AFP on and off in the same manner [see Eq. (13)] and would drop out when the slope difference $m_{off}-m_{on}$ was analyzed. However, the range of H fluxes used in this experiment had significant overlap between the AFP on and off conditions: for both the low- and high-field runs, $\gamma_H \approx 0.1$ to 0.35 sec^{-1} with AFP on, and $\gamma_H \approx 0.2$ to 0.7 sec^{-1} with AFP off. Thus the linearity of all the frequency versus γ_2 data for both AFP on and off (see Figs. 8–10) precludes a wall shift significantly nonlinear in the H density.

Indeed, a H-wall interaction consistent with both the experimental and theoretical results would probably entail a significant population of H atoms residing on the Teflon surface (i.e., physically adsorbed), yet remaining coherent with the bulk H ensemble and the maser oscillation. This would yield modified H_{bulk}-H_{wall} and H_{wall}-H_{wall} HI frequency-shift contributions, in addition to the H_{bulk}-H_{bulk} HI shift calculated by VKSLC. Such a possibility seems unlikely, however, given the known magnitude of the H adsorption energy on Teflon ($E_a \approx 143$ K) [67]. Assuming a simple, one-state physical adsorption model for the H-wall interaction, the bulk H density (n) and the surface H density (σ) are related by $\sigma = n\lambda_{th}\exp(E_a/k_BT)$ [12], where λ_{th} is the H thermal deBroglie wavelength. Therefore σ is very small near room temperature (~ 10 cm^{-2}) given typical H maser bulk H densities ($n \sim 10^9$ cm^{-3}), and so the rate of H_{bulk}-H_{wall} and H_{wall}-H_{wall} collisions would be very low. Note that such transient *physical adsorption* of H on Teflon should be distinguished from a "permanent" H-Teflon *chemical reaction* which may be responsible for the observed long-term wall degradation. Of course, any H that chemically reacts with the Teflon would cease to participate in the coherent H maser oscillation.

It is also possible that the present experiment had systematic errors in the corrections made to the raw frequency vs γ_2 data. These corrections included (i) the cavity frequency drift, (ii) the second-order Zeeman shifts due to changes in the static magnetic field, (iii) the wall degradation, and (iv) the MIS (at low fields). The cavity-induced frequency drift was determined in two ways: by monitoring the maser frequency drift for a day or more before and/or after a data-taking run; and by making several measurements of the "flux-tuned" cavity frequency, over a period of several months (see Fig. 5). The results of these two techniques agreed to 5–10% for the three data-taking runs reported here. (Note that the long-term measurement of the flux-tuned cavity frequency provides a far less precise determination of the maser frequency drift on the time scale of a day, mainly because of the freedom in choosing a function with which to fit the data.) Nonetheless, even a 10% change in the cavity-induced frequency drift rate would be far from sufficient to bring the experimental results for $\Omega_{on}-\Omega_{off}$ into agreement with the VKSLC theory. It seems unlikely, therefore, that inaccuracy in the cavity frequency drift correction was responsible for the discrepancy.

It is also unlikely that a systematic error in the second-order Zeeman shift correction was the culprit. For the low-field runs, we were able to correct for such Zeeman shifts down to the 0.1-μHz level. Also, drifts in the second-order Zeeman shift during maser frequency measurements were typically quite small (<2 μHz). During the high-field run, measurements by the "witness' maser (P28) and the flux-gate magnetometer showed no significant excursions of the internal and external static magnetic fields, respectively, at their level of sensitivity (~ 30 μHz). In addition, for all the data-taking runs, measurements were made by alternating the AFP on and off conditions. Thus for the high-field run it is improbable that slow, second-order Zeeman shift deviations of less than 30 μHz in magnitude could reconcile the observed $\Omega_{on}-\Omega_{off}$ behavior with the theory, as such drifts would tend to affect local sections of AFP on *and* off data rather than just all the on *or* all the off data.

We measured maser P27's wall degradation several times during a three-month period that included the three data-taking runs reported in the present paper. We found that running the maser at high H flux would accelerate the change of the density-independent contribution to the dephasing rate (γ_t), and that this degradation became progressively worse over a period of weeks. For the low-field runs the degradation was still relatively small ($\Delta\gamma_t \approx 0.01$ sec^{-1}); while about a month later, when the high-field run was performed, the degradation over the course of a run had increased to roughly 0.03 sec^{-1}. Nevertheless, the effect of such an increase in γ_t during a data-taking run was relatively minor, changing the derived value for $\Omega_{on}-\Omega_{off}$ by no more than 10% (see discussion in Sec. IV B). In addition, this correction acted to slightly *increase* the disagreement between our results and the VKSLC predictions. Therefore it is unlikely that wall degradation was the source of the discrepancy between theory and experiment.

Finally, there is the possibility of a systematic error in the correction for the MIS. As described in Sec. IV A above, we used the Reinhardt-Peters method [63] to measure the MIS in our low-field runs. The theoretical description of the MIS by Crampton and Wang (CW) [52,53] follows from the well-established Bloch-Wangsness-Redfield theory of density matrix relaxation in the presence of random perturbations [68–70] (originated for NMR studies), and is in very good agreement with previous MIS experimental investigations [52,53]. Hence the basic Reinhardt-Peters scheme of measuring the MIS by inverting the population difference $\rho_{dd}-\rho_{bb}$ [see Eq. (15)] should be a viable experimental technique. Therefore any systematic problem in our MIS measurement would have to have been due to reversals of the static field direction causing not only an inversion of $\rho_{dd}-\rho_{bb}$, but also a significant change in the distribution of transverse magnetic field gradients in the maser storage bulb. Our measurements consistently showed no significant difference between the γ_2 values for normal and inverted static fields, however, and from CW's MIS analysis this implies that the transverse magnetic field

gradients were in fact unchanged by the static field reversal. Also note that all our MIS measurements on maser P27, including test and trial runs as well as the low-field data-taking runs, found the magnitude of $\epsilon_m^{\rm off}$ to be in the range of 5.0 to 6.6×10^{-4}, and $\epsilon_m^{\rm on}$ to be typically a factor of 20 smaller. In addition, the comparable measured values for $\Omega_{\rm on}-\Omega_{\rm off}$ at high and low fields argue against there being a dominant systematic error in the low-field MIS correction, since there is no MIS at high fields.

Therefore we have not identified any sources of systematic error in our experiment that could explain the disagreement between the measurements of $\Omega_{\rm on}-\Omega_{\rm off}$ and the quantum-mechanical calculations of VKSLC. It may be worthwhile to repeat the room-temperature HI shift measurements using a different test maser, with possibly different Teflon wall coating properties or different magnetic gradient properties. This would also give better statistical certainty to the experimental results. We may be able to perform such further measurements at the CfA maser laboratory in the future; however, the limited availability of suitable H masers may preclude this possibility. On the other hand, there are two serious experimental efforts now underway that have been designed to measure HI shifts in low-temperature H masers. The CfA cryogenic H maser [8] will be operating again later this year, and should allow an investigation of HI effects for $T\sim0.5$ K. Also, Crampton [71] plans to measure H HI shifts near 10 K using a maser with a solid neon wall coating for its storage bulb. Together, these cryogenic measurements should give the VKSLC theory a definitive test, as the HI frequency shifts are predicted to be much larger at low temperature than at room temperature (see Fig. 3) and to depend much more sensitively upon unique aspects of the physics of cold atomic collisions (e.g., nonadiabatic effects).

VI. CONCLUSION

We have made atomic-hydrogen (H) maser frequency measurements, varying the incoming atomic population in the two masing states between approximately 100% (AFP on) and 50% (AFP off), in order to determine the change in the hyperfine-induced (HI) shift parameter Ω. Two different methods of maser operation (low and high fields) were employed in this work, and yielded comparable values for the HI shift parameter difference $\Omega_{\rm on}-\Omega_{\rm off}$. The measurements reported in the present paper indicate a dependence of Ω on the atomic hyperfine state populations, as predicted qualitatively by the quantum-mechanical (VKSLC) theory [26,27] [see Eq. (10) above]. However, both the magnitude and the sign of the measured value for $\Omega_{\rm on}-\Omega_{\rm off}$ disagree with the VKSLC calculations. We have not identified any sources of systematic error in the experiment that could explain this discrepancy.

With regard to the VKSLC theory, our experimental result is sensitive to the heretofore unmeasured HI frequency-shift cross section $\bar{\lambda}_1$, but is not sensitive to the cross section $\bar{\lambda}_2$, which is also predicted by the semiclassical theory [25] and is related to previous HI measurements [25,33]. Examining the calculational formulation for $\bar{\lambda}_1$ [72], it is possible that changes in the H-H interaction potentials used in the VKSLC computation could bring our results into agreement with theory. Further investigation of this possibility is warranted.

In summary, we draw the following conclusions from the measurements reported in the present paper: (i) there is a measurable dependence of the H HI spin-exchange frequency shift on the H hyperfine state populations, even at room temperature, which demonstrates the importance of including the hyperfine interaction in a proper theoretical treatment of H-H collisions; (ii) there is a significant nonlinear H density dependence to the total H spin-exchange frequency shift; (iii) given typical H maser values for $\gamma_{\rm H}$, the H flux must be kept stable to better than 5% to prevent HI shifts from limiting room-temperature maser fractional frequency stability at the 10^{-15} level (this is routinely achieved in existing H masers); (iv) the numerical VKSLC calculation of the HI frequency shift may be incomplete, perhaps only in that better H-H potentials are needed; and (v) it is, therefore, not yet justified to use the VKSLC calculations to predict the magnitude or the sign of the HI shifts in H masers at low temperatures. In the near term, our experimental investigations of HI spin-exchange frequency shifts in atomic hydrogen will concentrate on low-temperature measurements. This work should most directly provide information on the validity of the VKSLC theory and the importance of HI effects for new atomic frequency standards. It may also allow the study of important aspects of the unique physics of cold atomic collisions.

ACKNOWLEDGMENTS

We thank G. M. R. Winkler of the U.S. Naval Observatory for making masers P27 and P28 available for this experiment. We are grateful to B. J. Verhaar and H. T. C. Stoof for explaining their theoretical work to us and for allowing us to reproduce two of their figures in this paper. We also thank S. B. Crampton for useful discussions on all aspects of this subject. Financial support from DOE Grant No. DE-FG02-85ER45190 is acknowledged. One of us (R.W.) was supported by NASA.

*Current address: Harvard-Smithsonian Center for Astrophysics, Cambridge, MA 02138.

[1] A. A. Uljanov, N. A. Demidov, E. M. Mattison, R. F. C. Vessot, D. W. Allan, and G. M. R. Winkler, in *Proceedings of the 22nd Annual Precise Time and Time Interval (PTTI) Applications and Planning Meeting,* Vienna, VA, 1990 NASA Conf. Proc. 3116 (U.S. Naval Observatory, Washington, DC, 1990), p. 509.

[2] R. F. C. Vessot, M. W. Levine, E. M. Mattison, E. L. Blomberg, T. E. Hoffman, G. U. Nystrom, B. F. Farrell, R. Decher, P. B. Eby, C. R. Baugher, J. W. Watts, D. L. Teuber, and F. D. Willis, Phys. Rev. Lett. **45**, 2081 (1980).

[3] J. P. Turneaure, C. M. Will, B. F. Farrell, E. M. Mattison, and R. F. C. Vessot, Phys. Rev. D **27**, 1705 (1983).

[4] R. L. Walsworth, I. F. Silvera, E. M. Mattison, and R. F. C. Vessot, Phys. Rev. Lett. **64**, 2599 (1990).
[5] N. F. Ramsey, Rev. Mod. Phys. **62**, 541 (1990).
[6] H. F. Hess, G. P. Kochanski, J. M. Doyle, T. J. Greytak, and D. Kleppner, Phys. Rev. A **34**, 1602 (1986).
[7] M. D. Hürlimann, W. N. Hardy, A. J. Berlinsky, and R. W. Cline, Phys. Rev. A **34**, 1605 (1986).
[8] R. L. Walsworth, I. F. Silvera, H. P. Godfried, C. C. Agosta, R. F. C. Vessot, and E. M. Mattison, Phys. Rev. A **34**, 2550 (1986).
[9] S. B. Crampton, W. D. Phillips, and D. Kleppner, Bull. Am. Phys. Soc. **23**, 86 (1978).
[10] R. F. C. Vessot, M. W. Levine, and E. M. Mattison, in *Proceedings of the 9th Annual Precise Time and Time Interval (PTTI) Applications and Planning Meeting,* Goddard Space Flight Center, Greenbelt MD, 1977 (U.S. Naval Observatory, Washington, DC), p. 549.
[11] A. J. Berlinsky and W. N. Hardy, in *Proceedings of the 13th Annual Precise Time and Time Interval (PTTI) Applications and Planning Meeting,* Naval Research Laboratory, Washington, D.C., 1981 (U.S. Naval Observatory, Washington, DC 1981), p. 547.
[12] I. F. Silvera and J. T. M. Walraven, Phys. Rev. Lett. **44**, 164 (1980).
[13] E. M. Purcell and G. B. Field, Astrophys. J. **124**, 542 (1956).
[14] J. P. Wittke, Ph.D. thesis, Princeton University, 1955 (unpublished).
[15] J. P. Wittke and R. H. Dicke, Phys. Rev. **103**, 620 (1956).
[16] A. Dalgarno, Proc. R. Soc. London, Ser. A **262**, 132 (1961).
[17] P. L. Bender, Phys. Rev. **132**, 2154 (1963).
[18] L. C. Balling, R. J. Hanson, and F. M. Pipkin, Phys. Rev. **133**, A607 (1964); **135**, AB1 (1964).
[19] S. B. Crampton, Ph.D. thesis, Harvard University, 1964 (unpublished).
[20] S. B. Crampton, Phys. Rev. **158**, 57 (1967).
[21] S. B. Crampton, J. A. Duviver, G. S. Read, and E. R. Williams, Phys. Rev. A **5**, 1752 (1972).
[22] M. Desaintfuscien and C. Audoin, Phys. Rev. A **13**, 2070 (1976).
[23] D. Kleppner, H. M. Goldenberg, and N. F. Ramsey, Phys. Rev. **126**, 603 (1962).
[24] D. Kleppner, H. C. Berg, S. B. Crampton, N. F. Ramsey, R. F. C. Vessot, H. E. Peters, and J. Vanier, Phys. Rev. **138**, A972 (1965).
[25] S. B. Crampton and H. T. M. Wang, Phys. Rev. A **12**, 1305 (1975).
[26] B. J. Verhaar, J. M. V. A. Koelman, H. T. C. Stoof, O. J. Luiten, and S. B. Crampton, Phys. Rev. A **35**, 3825 (1987).
[27] J. M. V. A. Koelman, S. B. Crampton, H. T. C. Stoof, O. J. Luiten, and B. J. Verhaar, Phys. Rev. A **38**, 3535 (1988).
[28] E. Tiesinga, S. J. M. Kuppens, B. J. Verhaar, and H. T. C. Stoof, Phys. Rev. A **43**, 5188 (1991).
[29] E. Tiesinga, B. J. Verhaar, H. T. C. Stoof, and D. van Bragt, Phys. Rev. A **45**, 2671 (1992).
[30] S. Chu (private communication).
[31] J. L. Hall, M. Zhu, and P. Buch, J. Opt. Soc. Am. B **6**, 2194 (1989).
[32] M. Kasevich, E. Riis, S. Chu, and R. S. DeVoe, Phys. Rev. Lett. **63**, 612 (1989).
[33] G. A. Elkin and N. D. Zhestkova, Izmer. Tekh. **9**, 36 (1979).
[34] The Eindhoven group has subsequently included the Zeeman interaction in their analysis: A. C. Mann, H. T. C. Stoof, and B. J. Verhaar, Phys. Rev. A **41**, 2614 (1990). They found there to be small additional spin-exchange effects, of negligible magnitude except for static magnetic field strengths much greater than those typically used in H masers.
[35] R. M. C. Ahn, J. P. H. W. van den Eijnde, and B. J. Verhaar, Phys. Rev. B **27**, 5424 (1983).
[36] J. P. H. W. van den Eijnde, Ph.D. thesis, Eindhoven University of Technology, The Netherlands, 1984 (unpublished).
[37] A. M. Schulte and B. J. Verhaar, Nucl. Phys. **A232**, 215 (1974).
[38] L. Wolniewicz, J. Chem. Phys. **78**, 6173 (1983).
[39] J. F. Bukta and W. J. Meath, Mol. Phys. **27**, 1235 (1974).
[40] W. Kolos and L. Wolniewicz, Chem. Phys. Lett. **24**, 457 (1974).
[41] W. Kolos and L. Wolniewicz, J. Chem. Phys. **43**, 2429 (1965).
[42] W. Kolos, K. Szalewicz, and H. J. Monkhorst, J. Chem. Phys. **84**, 3278 (1986).
[43] D. Frye, G. C. Lie, and E. Clementi, J. Chem. Phys. **91**, 2366 (1989).
[44] P. R. Bunker, C. J. McLarnon, and R. E. Moss, Mol. Phys. **33**, 425 (1977).
[45] A. Dalgarno (private communication).
[46] B. J. Vehaar (private communication).
[47] A. C. Allison, Phys. Rev. A **5**, 2695 (1972).
[48] A. J. Berlinnsky and B. Shizgal, Can. J. Phys. **58**, 881 (1980).
[49] See Eqs. (55)–(60) in Ref. [26].
[50] W. N. hardy, M. Morrow, R. Jochemsen, B. W. Statt, P. R. Kubik, R. M. Marsolais, A. J. Berlinsky, and A. Landesman, Phys. Rev. Lett. **45**, 453 (1980).
[51] J. Vanier and C. Audoin, *The Quantum Physiccs of Atomic Frequency Standards* (Hilger, Bristol, 1989).
[52] S. B. Crampton and H. T. M. Wang, in *Proceedings of the 28th Annual Symposium on Frequency Control,* Atlantic City, NJ, 1974 (Electronics Industries Association, Washington, DC, 1974), p. 355.
[53] S. B. Crampton, in *Proceedings of the 2nd Frequency Standards and Metrology Symposium,* Copper Mountain, CO, 1976 (National Institute of Standards and Technology, Boulder, CO, 1976), p. 589.
[54] E. M. Mattison, R. F. C. Vessot, and W. Shen, IEEE Trans. Ultra. Ferro. Freq. Contr. **UFFC-34**, 622 (1987).
[55] For N measurements x_i, with a mean value $\bar{x}$ and assuming an equal Gaussian distribution of uncertainties for all x_i, the "estimated error of the mean" is equal to $[N(N-1)]^{-1}\sum_i (x_i-\bar{x})^2$. See P. R. Bevington, *Data Reduction and Error Analysis for the Physical Sciences* (McGraw-Hill, New York, 1969), p. 70.
[56] D. Allan, Proc. IEEE **54**, 105 (1966).
[57] T. K. Peppler and D. W. Allan (private communication).
[58] Teflon FEP-120 is a fluorinated ethylene-propylene resin. Teflon is a trademark of E. I. duPont de Nemours and Co., Inc.
[59] E. M. Mattison, R. F. C. Vessot, and C. Bain, S. Wasserman, and G. Whitesides, in *Proceedings of the 41st Annual Symposium on Frequency Control,* Philadelphia, PA, 1987 (IEEE Publishing Services, New York, NY 1987), p. 95.
[60] Zerodur is a trademark of Schott Optical Glass, Inc.
[61] S. F. Jacobs, in *Proceedings of the 2nd Frequency Standards and Metrology Symposium,* Copper Mountain, CO,

1976 (available from National Institute of Standards and Technology, Boulder, CO, 1976), p. 269.
[62] Cer-Vit C101 was manufactured by Owens-Illinois, Inc. in the 1970s. The formula and manufacturing rights were subsequently sold to Schott Optical Glass, Inc., who have since declined to produce any of the material.
[63] V. S. Reinhardt and H. E. Peters, in *Proceedings of the 29th Annual Symposium on Frequency Control,* Atlantic City, NJ, 1975 (Electronics Industries Association, Washington, DC, 1975), p. 357.
[64] Tests needed to be performed on SAO maser P28 in preparation for its shipment to the U.S. Naval Observatory, per contractual obligations.
[65] H. G. Andresen, Z. Phys. **210**, 113 (1968).
[66] A numerical tabulation of the VKSLC results, graphically displayed in Ref. [26], has been provided to us by Professor B. J. Verhaar.
[67] R. F. C. Vessot, E. M. Mattison, E. A. Imbier, and Z. C. Zhai, in *Proceedings of the 16th Annual Precise Time and Time Interval (PTTI) Applications and Planning Meeting,* Goddard Space Flight Center, Greenbelt, MD, 1984 (U.S. Naval Observatory, Washington, DC, 1984), p. 357.
[68] R. K. Wangsness and F. Bloch, Phys. Rev. **89**, 728 (1953).
[69] F. Bloch, Phys. Rev. **102**, 104 (1956).
[70] A. G. Redfield, IBM J. Res. Dev. **1**, 19 (1957).
[71] S. B. Crampton (private communication).